small methods
www.small-methods.com

Organic Upgrading through Photoelectrochemical Reactions: Toward Higher Profits

Tae-Kyung Liu, Gyu Yong Jang, Sungsoon Kim, Kan Zhang, Xiaolin Zheng,* and Jong Hyeok Park**

Aqueous photoelectrochemical (PEC) cells have long been considered a promising technology to convert solar energy into hydrogen. However, the solar-to-H_2 (STH) efficiency and cost-effectiveness of PEC water splitting are significantly limited by sluggish oxygen evolution reaction (OER) kinetics and the low economic value of the produced O_2, hindering the practical commercialization of PEC cells. Recently, organic upgrading PEC reactions, especially for alternative OERs, have received tremendous attention, which improves not only the STH efficiency but also the economic effectiveness of the overall reaction. In this review, PEC reaction fundamentals and reactant-product cost analysis of organic upgrading reactions are briefly reviewed, recent advances made in organic upgrading reactions, which are categorized by their reactant substrates, such as methanol, ethanol, glycol, glycerol, and complex hydrocarbons, are then summarized and discussed. Finally, the current status, further outlooks, and challenges toward industrial applications are discussed.

1. Introduction

As energy demands and environmental crises continue to grow, renewable energy has drawn much attention in recent years. The use of fossil fuels, such as coal, oil, and natural gas, emits CO_2, contributing to climate change by greenhouse effects. On the other hand, renewable energy sources, such as light, wind, and hydropower, barely produce pollutants; thus, these sources provide a sustainable solution to future energy demands and help keep the environment clean. This is especially important as societies worldwide seek to reduce their carbon footprint and mitigate the effects of climate change. Moreover, renewable energy sources can be used over centuries without depleting the Earth's natural resources.

Among the renewable energy sources, light energy is one of the ultimate renewable energies, as an infinite amount of light reaches Earth directly from the Sun. Photoelectrochemical (PEC) cells are a type of electrochemical cell that absorbs light energy to generate an electrical potential that drives the chemical reaction.[1–8] One of the main advantages of PEC cells is their efficiency, as they allow a significant portion of light energy to be converted into high-energy electrons and holes, which can be used to operate chemical reactions. This high efficiency makes PEC cells particularly useful, as light energy can be precisely controlled to regulate the reaction rate and product yield. Another remarkable feature of PEC cells is that compared to other existing chemical processes, they occur in relatively mild conditions.[9,10] This is because most commercialized chemical processes require high temperatures and pressure, which causes significant energy loss in the overall process. On the other hand, PEC cells are operated at room temperature and low pressure, making them highly economic. Moreover, the high temperature of the chemical processes is generated from the steam boiler by burning fossil fuels, which emit a significant amount of CO_2, while the PEC reactions do not emit any kind of pollutants during the overall reaction process.

Traditional PEC cells achieve hydrogen production from the water-splitting reaction, which was first developed by Fujishima and Honda in 1972.[11] In the case of the water splitting reaction, the hydrogen evolution reaction (HER) and oxygen evolution reaction (OER) mainly occur at the cathode and anode in the electrochemical cell, respectively; in this process, the light-harvesting photoelectrode is adapted in either the cathode or anode, which are denoted as the photocathode or photoanode, respectively.[12–15] Even though hydrogen production by PEC water splitting has been known as the ultimate clean energy production system that converts light energy into hydrogen molecules, the development of water splitting encounters many difficulties in increasing its efficiency, especially due to the poor kinetics of the OER.[16–20] The OER utilizes a four-electron transfer

T.-K. Liu, G. Y. Jang, S. Kim, J. H. Park
Department of Chemical and Biomolecular Engineering
Yonsei University
Seodaemun-gu, Seoul 03722, Republic of Korea
E-mail: lutts@yonsei.ac.kr
S. Kim, X. Zheng
Department of Mechanical Engineering
Stanford University
Stanford, CA 94305, USA
E-mail: xlzheng@stanford.edu
K. Zhang
School of Materials Science and Engineering
Nanjing University of Science and Technology
Nanjing 210094, P. R. China
E-mail: zhangkan@njust.edu.cn

The ORCID identification number(s) for the author(s) of this article can be found under https://doi.org/10.1002/smtd.202300315

DOI: 10.1002/smtd.202300315

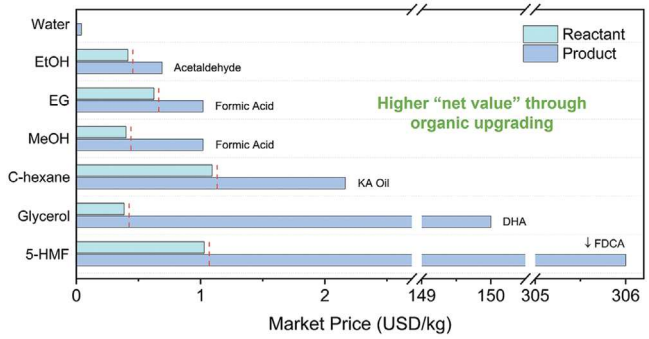

Figure 1. Schematic illustration showing the market price of representative products for each organic upgrading reactant discussed in this work. Red lines represent the calculated price of products when they are assumed to have the same "net value" as the OER. C-Hexane: cyclohexane, HMF: 5-hydroxymethylfurfural, DHA: 1,3-dihydroxyacetone, FDCA: 2,5-furandicarboxylic acid.

mechanism that requires a high overpotential and exhibits poor kinetics.[21–25] Moreover, photoelectrodes are often degraded during the OER due to the self-oxidation of the electrode by the exciton.[26–28] Therefore, some researchers have proposed alternatives to alter PEC water oxidation into other oxidation reactions, such as organic upgrading, H_2O_2 production, and chloride ion oxidation.[29–35]

PEC upgrading reactions are advantageous than two other catalytic reactions, photocatalysis (PC) and electrocatalysis (EC). These catalytic reactions convert energy in different ways and exhibit distinctive catalytic features which can lead to the upgrade of chemicals by generating strong oxidizing hydroxyl radicals to achieve the oxidation through multiple reaction steps. In detail, PC is considered to be a technique with great potential due to its environmentally friendliness and its ability to save energy. However, it has some limitations such as the inability to upgrade chemicals at high concentrations which hampers its application. In addition, semiconductor materials usually used for PC are prone to photocorrosion, causing photogenerated electron–hole pairs to combine easily, resulting in low quantum efficiencies.

On the other hand, EC has higher energy efficiency, and can be easily operated on smaller working area, wider pH range, and with stronger oxidation ability. However, during EC reactions, initial reactants and intermediate products can easily accumulate on the surface of the electrode, blocking the active sites leading to electrode instability. Therefore, above drawbacks greatly limit the application of PC and EC in organic upgrading, which made PEC reactions become a topic of increasing interest as a promising method to upgrade chemicals into value-added products.

Among various PEC reactions, oxidative organic upgrading has drawn attention recently. Most of the organics for PEC reactions are readily oxidized at potentials lower than the standard water oxidation potential, resulting in higher performance of PEC cells in terms of onset potential, photocurrent density, and long-term stability.[36–39] Because PEC organic upgrading involves either alternating poor water oxidation or value-addition of organic molecules, the prices of organic products are generally higher than those of chemicals before upgrading reactions. As shown in **Figure 1**, the current price of oxygen is approximately 0.04 USD kg^{-1}, while the price of formic acid, which is among the most reported products from organic upgrading, is over a thousand times higher (up to 110 USD kg^{-1}). Moreover, comparing the price of the reactant and product materials demonstrates that organic upgrading by the PEC reaction is highly feasible from an economic point of view and that the counterpart H_2 evolution reaction HER is still highly useful. Considering the performance enhancement in PEC systems with new oxidation reactions, organic upgrading will be a more cost-effective reaction compared to the OER.

In this review article, various kinds of organic upgrading by the PEC process are introduced comprehensively. First, the fundamentals of PEC organic upgrading, including working principles, economic considerations, and applications, are demonstrated in detail. Next, recent progress in PEC organic upgrading is introduced with several categories of reactants, such as methanol, ethanol, glycol, glycerol, and complex hydrocarbons. Finally, the remaining challenges and future aspects for PEC organic upgrading are discussed. We believe that the PEC organic upgrading reaction shows remarkable potential to solve current energy and environmental issues owing to its environmental friendliness and efficiency, which will lead the future chemical process and market.

2. Fundamentals of Photoelectrochemical Organic Upgrading

2.1. Fundamentals of Photoelectrochemistry

Understanding semiconductor photoelectrodes is crucial for comprehending PEC technology. When a semiconductor is illuminated with photons with energies higher than their bandgap (indicating that the electrons have sufficient energy to travel from the valence band to conduction band), "excited electron" and "hole" pairs in the conduction and valence bands are formed, respectively.[8] Once the thermodynamically favorable band structure is formed, such photogenerated charge carriers can travel to the semiconductor surface to participate in the oxidation and reduction reactions. When a semiconductor is immersed in the electrolyte, electron transfer between the semiconductor surface and the electrolyte occurs to equilibrate its Fermi level with the redox potential of the electrolyte.[40] As shown in **Figure 2**, when the redox potential of the electrolyte is more negative (positive) than the Fermi level of the semiconductor, electrons travel from (to) the electrolyte solution to (from) the semiconductor. Due to the fixed energy level at the surface and the altered Fermi level, such charge migration causes "band bending" at the semiconductor surface.[40] Additionally, transfer of charges from (to) the electrochemically neutral semiconductor causes an imbalance of charges at the semiconductor surface, leading to the formation of the space charge region (SCR). Taking an n-type semiconductor as an example, the built-in electric field formed by the charge imbalance and the resulting SCR causes holes to travel toward the surface and participate in oxidation reactions, whereas the electrons travel to the cathode through the external circuit to participate in reduction reactions (and vice versa for a p-type semiconductor). The band structure of the photoelectrodes must be adequately positioned to thermodynamically drive redox reactions. The valence band maximum (VBM) of an n-type semiconductor

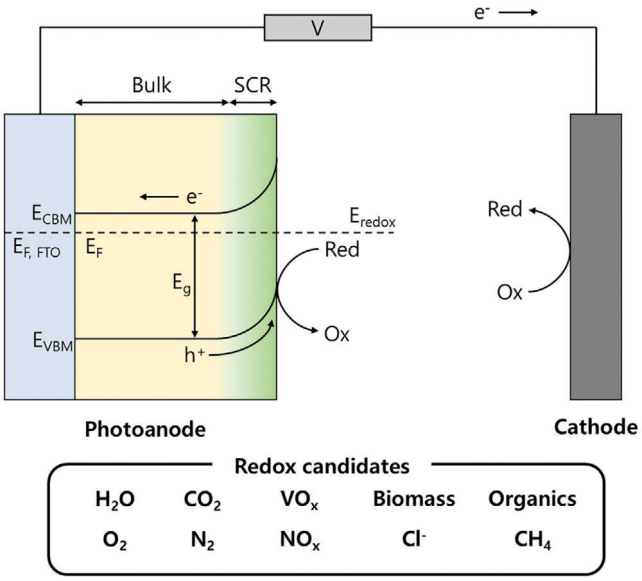

Figure 2. Schematic illustration of the PEC reaction process and redox candidates on semiconductor photoanodes. Red: reduction, Ox: oxidation, SCR: space charge region, E_{CBM}: energy of conduction band minimum, E_{VBM}: energy of valence band maximum, E_g: bandgap energy, E_F: Fermi level of photoanode.

must be more positive than the redox potential of oxidation reactions, and the conduction band minimum (CBM) must be more negative than the redox potential of reduction reactions. Additionally, to overcome thermodynamic barriers of the redox reaction, the band gap of the semiconductor must exceed the sum of the theoretical redox potential and the activation overpotential for both oxidation and reduction reactions.

2.2. Advantages of Photoelectrochemical Organic Upgrading Reactions

Generally, the water-splitting reaction consists of the following reactions: an oxidation reaction to produce O_2 molecules (OER) and a reduction reaction to produce H_2 molecules (HER). As in Equations 1 and 2, two electrons are needed to produce one H_2 molecule, and four are needed to produce one O_2 molecule.

$$\text{OER}: 2H_2O + 4h^+ \rightarrow O_2 + 4H^+ \quad (1)$$

$$\text{HER}: 2H^+ + 2e^- \rightarrow H_2 \quad (2)$$

$$\text{Overall water splitting}: \quad 2H_2O + 2H_2 \rightarrow O_2 \quad (3)$$

Overall water splitting is an uphill reaction with a standard free energy change ($\Delta G°$) of 237.2 kJ mol^{-1}, which corresponds to a theoretical redox potential of 1.23 V. However, as described above, sluggish OER kinetics lead to large activation overpotentials. Considering activation overpotentials, ohmic losses, and other minor losses, the actual minimum energy needed for a semiconductor to drive the water-splitting reaction is proposed to be approximately 2.3 eV.[20,41] Additionally, O_2 produced from OER possesses low economic value, with an average market price of 0.04 USD kg^{-1}.[42] Such sluggish kinetics and the low economic value of OER reactions limit the overall economic value of the water-splitting system. Although hole scavengers (sodium sulfite, hydrogen peroxide, etc.) or sacrificial organic reactants (urea, methanol, ammonia, etc.) were introduced to improve the oxidation kinetics, they often result in the production of undesired, invaluable products, such as CO_2 or NO_2.[43] Therefore, developing substitute reactions with high economic value is crucial to ensure the economic feasibility of PEC reactions.

Over recent years, many value-adding reactions have been studied as a substitute for the OER, such as the production of hydrogen peroxide or oxidizing reagents ($S_2O_8^{-}$, HClO, etc.). However, organic synthesis reactions, especially "organic upgrading" reactions in which the product's economic value is higher than that of the reactant's, are highly intriguing and worth exploring for the following reasons: 1) They proceed under mild and less-demanding conditions. Industrial organic synthesis reactions proceed under harsh (high temperature and pressure) and toxic conditions, which is far from environmentally friendly and is also economically unsatisfactory. However, PEC organic upgrading reactions mostly proceed under room temperature and pressure conditions, and some reactions even proceed under aqueous electrolyte conditions, which eliminates the need for toxic organic solvents. Light illumination also significantly reduces the needed reaction overpotential, making them even greener and less demanding. 2) They can generate a high reaction "net value." Even though organic upgrading reactions require feed streams of organic molecules, when calculating the value produced from the reaction, the value difference between the reactant and the product (the "net value") is what truly matters. From this viewpoint, as shown in Figure 2, organic upgrading reactions boost the value of reactants to produce high-value products, meaning that they possess a high net value. For example, as shown in Figure 1, when glycerol is converted into 1,3-dihydroxyacetone, they produce a net value of ≈148.9 USD kg^{-1}, which is over 3700 times higher than that of water splitting reactions (≈0.04 USD kg^{-1}). 3) They have a wide range of applications. The development of PEC strategies toward value-added production will frequently be aimed toward a single specific product. However, for organic upgrading reactions, the development of a single strategy to activate or convert a specific organic bond can be applied to many organic substrates. For example, Zhao et al. developed a universal oxygen-atom transfer PEC catalyst and carried out various transformations, such as sulfoxidation, C=C epoxidation, oxygenation of Ph_3P and monooxygenation of inorganic ions.[44] Similarly, Li et al. developed a universal PEC C-H halogenation strategy, which could be applied to 27 substrates.[45] Such wide applicability and versatile product range of organic upgrading reactions can extend the role of PEC reactions beyond energy conversion/storage technology toward a practical and useful tool to replace industrial synthetic methods.

Inspired by the intriguing features described above, this review aims to summarize recent progress and developments achieved in organic synthesis reactions. Special emphasis is placed on "organic upgrading" reactions, in which the product's economic value is higher than that of the reactant. Reactions will be classified according to their reactants and will be divided into the

following sections: alcohols and complex hydrocarbons. Finally, the current status and future outlook of organic upgrading reactions will be briefly discussed.

3. Photoelectrochemical Organic Upgrading

3.1. Alcohols

3.1.1. Methanol

Methanol, the simplest alcohol, can be derived from a variety of carbon resources, including natural gas, biomass, coal, and CO_2, and is often used as a hole scavenger to increase H_2 production in electrochemical reactions.[46–48] As a basic byproduct of petrochemical manufacturing, methanol has a low market price (0.40 USD kg^{-1}).[49] Therefore, the oxidation of methanol to formaldehyde and formic acid is a value-added process because of the market price of formaldehyde (0.43 USD kg^{-1}) and formic acid (≈110 USD kg^{-1} for 95%) is higher than that of methanol.[50,51] Methanol oxidation has a low oxidation potential (0.03 V vs NHE) compared to the water oxidation potential (1.23 V vs NHE), which makes methanol oxidation thermodynamically more favorable.[52] PEC methanol oxidation has recently been studied extensively along with H_2 generation, and many works have suggested possible mechanisms for methanol oxidation into products such as formaldehyde, formic acid, and CO_2.[53]

As hydroxyl ions are very efficient hole scavengers, the pathway for methanol oxidation differs in different pH values of the reaction media.[54] For neutral or acidic media, in which the number of hydroxyl ions is very small, methanol and its intermediates are expected to react directly with the holes generated in semiconductor photoanodes excited by absorption of photons, as in Equations 4– 6; in basic media, in which the number of hydroxyl ions is sufficiently large, photogenerated holes will react with hydroxyl ions to form hydroxyl radicals, which in turn react with methanol and its intermediates for the oxidation reaction, as shown in Equations 7 and 8.
Neutral or acidic media:

$$CH_3OH + 2h^+ \rightarrow HCHO + 2H^+ \quad (4)$$

$$HCHO + H_2O + 2h^+ \rightarrow HCOOH + 2H^+ \quad (5)$$

$$HCOOH + 2h^+ \rightarrow CO_2 + 2H^+ \quad (6)$$

Basic media:

$$6OH^- + 6h^+ \rightarrow 6OH^* \quad (7)$$

$$CH_3OH + 6OH^* \rightarrow CO_2 + 5H_2O \quad (8)$$

Methanol oxidation pathways, other than those mentioned above, can be possible depending on the electron donor ability of intermediates. For instance, because one of the intermediates of methanol oxidation, typically formaldehyde, is a stronger electron donor than water, oxidation of formaldehyde could occur by direct interaction with the holes rather than through the water splitting reaction.[54]

Formaldehyde, one of the main products of methanol oxidation, is an important raw material and is widely used in industrial chemical products, such as resins, pesticides, and anticorrosion reagents.[55,56] The annual demand for formaldehyde has surpassed 30 megatons, and the production of formaldehyde has been extremely stable.[57,58] As demand for cosmetics, disinfectants, and pharmaceuticals increases, the demand for formaldehyde is expected to grow continuously with the manufacturing industry's development.[59] Formaldehyde is conventionally synthesized by the oxidation of methanol at extremely high temperatures using various metal and oxide catalysts.[60] Therefore, PEC methanol oxidation to produce formaldehyde has drawn much attention owing to its environmental friendliness and sustainability.

In 1984, Osaka et al. first reported PEC methanol oxidation to formaldehyde using an Fe_2O_3/n-Si heterojunction electrode.[61] The photocurrent increased by a ratio of 1.25 in the presence of 0.6 M methanol compared to the photocurrent without methanol. To determine whether methanol was photoelectrochemically oxidized to formaldehyde, the electrolyte after 10 h of electrolysis at 3.0 V versus Hg/HgO in a 0.2 M KOH solution under illumination was analyzed by gas chromatography (GC). Although the exact amount of production or the possibility of further oxidation of formaldehyde was not discussed, formaldehyde was shown to be produced as a main liquid product. Marugán et al. reported a TiO_2 P25 photoanode as an active system for the PEC oxidation of methanol and used colorimetric determination according to Nash's method to evaluate the formaldehyde produced during the reaction.[62,63] Similarly, Haisch et al. employed the same method to show that formaldehyde was the main product of methanol oxidation on both cold-sprayed TiO_2 and WO_3 photoanodes.[64]

Mesa et al. reported kinetic and mechanistic analyses for selective methanol oxidation to formaldehyde on TiO_2 and α-Fe_2O_3 photoanodes under PEC conditions.[65] They suggested that in both types of photoanodes, the oxidation of methanol is a second-order reaction with respect to surface accumulated holes. To confirm this, they plotted the photocurrent density (J_V) as a function of the surface hole density (p_s) for methanol oxidation on TiO_2 and α-Fe_2O_3 photoanodes. As a result, the gradients of $\log(J_V)$ versus $\log(p_s)$ for all datasets were close to 2 with little variation. Furthermore, by comparing the J_V and p_s datasets at different applied potentials, the kinetics of the methanol oxidation reaction were shown to be dependent on the metal oxide surface chemistry but independent of the applied potential (**Figure 3**a). This also suggests that the kinetics of the reaction are determined by the density of holes accumulated at the electrode surface, in which the energy is determined by the valence band potential and not by the electrode's Fermi level or band bending. When comparing the PEC methanol oxidation performance of the two photoanodes, TiO_2 was at least two orders of magnitude faster than α-Fe_2O_3. This further supported that the kinetics of the methanol oxidation reaction are dependent on the valence band potential because the valence band potential of TiO_2 is more positive than that of α-Fe_2O_3. They also revealed that the rate-limiting step of PEC methanol oxidation is the cleavage of the C–H bond by analyzing the kinetic isotope effects.

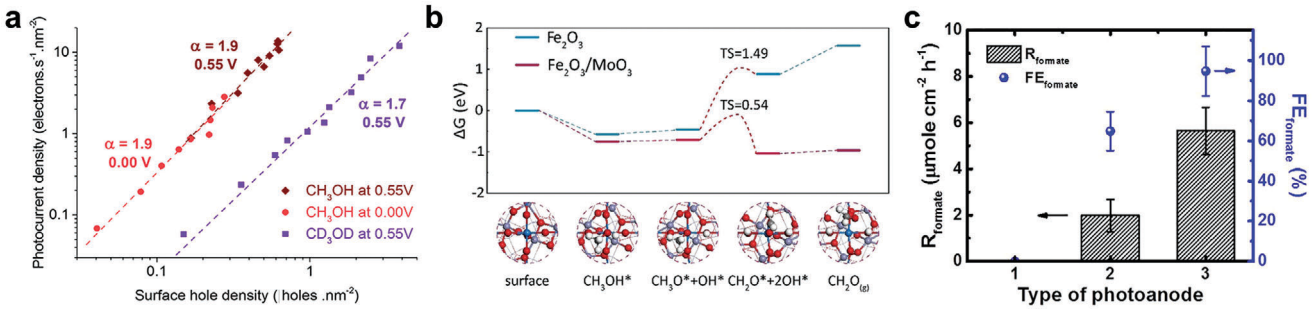

Figure 3. a) Rate law analysis, photocurrent density, $J_{holes}{}^{sur}$, and surface hole density, dp_s, of the oxidation of methanol on α-Fe_2O_3 at 0.55 V (dark red) and 0.00 V (light red) and TiO_2 (blue) at −0.80 V applied potentials. Reproduced with permission.[65] Copyright 2017, American Chemical Society. b) Calculated free energy profiles for the formox process on Fe_2O_3 and Fe_2O_3/MoO_3. Reproduced with permission.[68] Copyright 2021, Wiley-VCH. c) Formate generation rate ($R_{formate}$) and $FE_{formate}$ from 2 h PEC methanol reforming at the pristine $BiVO_4$ (#1) $BiVO_4$|nanoNi-Bi (#2), and $BiVO_4$|nanoFe:Ni-Bi (#3) photoanodes. Reproduced with permission.[75] Copyright 2020, Elsevier.

A number of researchers have attempted to enhance the activation of this C–H bond by either engineering the morphology or by constructing a heterojunction. Berger et al. designed TiO_2 nanowire photoanodes to maximize formaldehyde production due to the short distance between the generated methoxy radicals and the neighboring TiO_2 nanowires.[66] Zheng et al. decorated Au on ZnO/α-Fe_2O_3 nanotube arrays to offer efficient and stable PEC methanol oxidation into formaldehyde.[67] Along with the plasmonic effect of Au nanoparticles, the aligned and porous structure of ZnO/α-Fe_2O_3/Au nanotube arrays contributed to an improvement in faradaic efficiency (FE) of 79.23% compared with 28.77% for pristine ZnO nanorod arrays. Huang et al. constructed a Z-scheme Fe_2O_3/MoO_3 hollow nanotube with a methanol to formaldehyde selectivity of 95.7%.[68] DFT calculations revealed that the high selectivity toward formaldehyde was due to faster C–H bond breaking kinetics with more favorable methanol adsorption and formaldehyde dissociation for Fe_2O_3/MoO_3 heterojunctions, which could also enhance the photochemical conversion efficiency by constructing an internal electric field (Figure 2b). Recently, the same group also synthesized g-C_3N_4 and $CoFe_2O_4$ to construct a heterojunction with α-Fe_2O_3 nanotube arrays.[69,70] Both works showed improved PEC activity owing to increased electron transfer by the heterojunction with formaldehyde selectivities of 81.5% and 97.8%, respectively. For the α-Fe_2O_3/g-C_3N_4 hybrid, the N atoms with higher electronegativity than the O atoms were responsible for C–H bond activation, whereas for the α-$Fe_2O_3/CoFe_2O_4$ hybrid, the lower adsorption energy for methanol on $CoFe_2O_4$ enhanced the activation of C–H bonds, resulting in high selectivity for formaldehyde production.

Formic acid, which can also be produced by methanol oxidation, is widely used in the chemical, agricultural, leather, pharmaceutical, textile, and rubber industries. The annual worldwide production capacity of formic acid was estimated to be approximately 950 tons.[71] The demand for formic acid is also growing owing to its relatively noncorrosive and nontoxic properties, which allow formic acid to be easily handled.[72] In addition, formic acid is currently among the most promising candidates for storing hydrogen due to its high volumetric capacity and its low flammability under ambient conditions.[73]

Lin et al. demonstrated the capability of the α-Fe_2O_3/NiBi photoanode in PEC methanol oxidation to formate.[74] Under light illumination, an FE of 77.5% for formate production was detected for the α-Fe_2O_3/NiBi photoanode compared with the low FE (≈5%) for the pristine α-Fe_2O_3 photoanode. However, samples were examined at relatively high potentials (1.48 V vs RHE), in which very little work was performed by light illumination.

Huang et al. investigated PEC methanol oxidation to formic acid at near-neutral pH conditions with an electrosynthesized nickel–iron oxyhydroxide–borate nanoparticulate thin film (nanoFe:Ni-Bi).[75] They first optimized the electrocatalytic performance to produce formic acid from methanol oxidation by doping Fe into a nanoporous nickel oxyhydroxide–borate thin film (nanoNi–Bi). The presence of Fe promoted the formation of Ni^{3+} active species, which improved the methanol oxidation kinetics. After optimization, nanoNi–Bi and nanoFe:Ni–Bi were integrated with $BiVO_4$ to deliver a higher photocurrent response, and the formate generation rate was analyzed at a bias of 0.55 V versus RHE in borate buffer (0.1 M, pH 9.4) containing 0.1 M methanol. The $BiVO_4$/nanoFe:Ni–Bi photoanode exhibited an increased formate generation rate of 5.7 μmol cm^{-2} h^{-1} with an FE of 94.6%, whereas the $BiVO_4$/nanoNi–Bi catalyst showed a lower formate generation rate of 2.0 μmol cm^{-2} h^{-1} and an FE of 64.8% (Figure 3c). Overall, an effective electrocatalyst was able to transform an inactive $BiVO_4$ photoanode into a highly efficient and selective photoanode for PEC methanol oxidation to formic acid at lower applied potentials.

3.1.2. Ethanol

Ethanol, which is mostly produced from corn biomass through ethanol fermentation and distillation, is becoming an important link between biomass and renewable fuels and chemicals.[76] The produced ethanol is mostly used by blending into gasoline as a renewable fuel, but it can also be transformed into value-added chemicals, such as acetaldehyde, diethyl ether, acetic acid, acetone, and ethyl acetate.[77] Similar to methanol, ethanol is also used as a hole scavenger in PEC water-splitting systems to increase H_2 production, and the oxidation of ethanol leads to the formation of acetaldehyde.[78–80] The oxidation of ethanol to acetaldehyde is a value-adding process because the market price of acetaldehyde (0.69 USD kg^{-1}) is over 1.5-fold higher than the market price of ethanol (0.42 USD kg^{-1}).[81,82]

Ethanol oxidation is a multielectron transfer reaction, and a number of products can be generated in the process, including acetaldehyde and acetic acid. The oxidation of ethanol progresses to acetaldehyde, acetic acid, and CO_2 as a final product. In detail, after the formation of acetaldehyde (Equation 9), the reaction can either lead to the production of acetic acid followed by methane (Equations 10 and 11), or it can involve the production of CO_2 to release protons (Equation 12). The reaction pathways of ethanol oxidation also vary with different pH conditions (Equations 13 and 14), and the selectivity of the product is mostly related to the pH of the electrolyte and the selected electrode.[54]

Neutral or acidic media:

$$C_2H_5OH + 2h^+ \rightarrow CH_3CHO + 2H^+ \quad (9)$$

$$CH_3CHO + H_2O + 2h^+ \rightarrow CH_3COOH + 2H^+ \quad (10)$$

$$CH_3COOH \rightarrow CH_4 + CO_2 \quad (11)$$

$$CH_3CHO + 3H_2O + 10h^+ \rightarrow 2CO_2 + 10H^+ \quad (12)$$

Basic media:

$$12OH^- + 12h^+ \rightarrow 12OH^* \quad (13)$$

$$C_2H_5OH + 12OH^* \rightarrow 2CO_2 + 9H_2O \quad (14)$$

Although some researchers have reported products other than acetaldehyde, such as 2,3-butanediol, are generated from PEC ethanol oxidation, most of the works reported acetaldehyde as the main liquid product.[83] Ampelli et al. designed an Au-modified TiO_2 nanotube array-based photoanode for PEC ethanol oxidation, in which they mainly investigated the effect of gold nanoparticles on hydrogen production.[84] The main product for PEC ethanol oxidation was acetaldehyde, and the process prevailed over the reaction of complete ethanol reforming to afford CO_2. An Au-modified TiO_2 nanotube array was first evaluated as a photocatalyst, and the selectivity of the reaction to acetaldehyde was remarkably high (98%), suggesting a good example of solar-driven chemistry. The group further designed it into a PEC cell, and the Au-modified TiO_2 nanotube array showed 1.5-fold higher H_2 production in the presence of ethanol compared with that of the bare TiO_2 nanotube array without gold nanoparticles.

Boltersdorf et al. studied the adsorption and desorption characteristics of ethanol and its intermediates as a key factor in improving the selectivity of the product with gold–palladium (Au–Pd) bimetallic nanostructure catalysts.[85] They reported efficient PEC ethanol oxidation into acetaldehyde and CO_2 at low temperatures with Au–Pd nanoparticles on TiO_2 supports. Au nanostructures are known to exhibit localized surface plasmon resonance (SPR), which promotes the generation of hot electrons for catalytic reactions. By constructing an Au–Pd alloy, the generated hot electrons could flow to the surface of Pd, which acts as an active center for reactions, specifically ethanol oxidation, to participate in the reaction. For photocatalytic ethanol oxidation, the core-shell structure Au–Pd alloy with 10% Pd showed the highest acetaldehyde production with 1.06 μmol g^{-1} catalyst, but product analysis for PEC ethanol oxidation was not available.

Yuan et al. reported highly selective PEC ethanol oxidation to acetaldehyde with nearly 100% selectivity with an α-Fe_2O_3 photoanode and revealed the reaction mechanism by operando spectroelectrochemistry.[86] In detail, photogenerated holes in α-Fe_2O_3 during PEC ethanol oxidation and acetaldehyde oxidation were investigated using operando spectroelectrochemical photoinduced absorption spectroscopy (PIA) and transient photocurrent (TPC) techniques under quasi-steady state conditions. First, the onset potential, which was shifted in the cathodic direction in the presence of ethanol, suggested that a favorable hole transfer pathway functions as a hole scavenger. Compared to the photocurrent in the ethanol electrolyte, the photocurrent in the acetaldehyde electrolyte shows a negligible photocurrent, indicating that the PEC acetaldehyde oxidation reaction is more challenging to perform than the PEC ethanol oxidation reaction. When the product of PEC ethanol oxidation reactions was determined, only acetaldehyde was detected with a negligible amount of oxygen, showing highly selective acetaldehyde formation on the α-Fe_2O_3 photoanode. The activation barrier of acetaldehyde oxidation (398 meV) was higher than that of ethanol oxidation (195 meV), supporting the apparent high selectivity of acetaldehyde formation with the suppression of further oxidation into other products. Overall, the sluggish acetaldehyde oxidation on the α-Fe_2O_3 photoanode and the 0.5^{th} reaction order in holes due to the high activation barrier and mass transport limited by the surface adsorption of aldehyde molecules provided a significant advantage for the highly selective green synthesis of acetaldehyde by PEC ethanol oxidation.

3.1.3. Glycol

Ethylene glycol (EG), the simplest glycol, is an important organic chemical intermediate used in a vast number of industrial processes, such as energy, plastics, and automobiles. Owing to the unique and versatile applications of EG, a variety of catalytic and noncatalytic chemical systems have been studied to synthesize EG, particularly by reaction processes from fossil fuels and resources from biomass.[87] PEC oxidation of EG has recently gained interest from researchers who are seeking efficient strategies to recycle polyethylene terephthalate (PET) plastic wastes to useful products. This is because PET plastic can be easily hydrolyzed to release water-soluble ethylene glycol and terephthalic acid monomers.[88,89] A PET upcycling process using PET hydrolysis toward value-added chemicals has been successfully achieved by nonnoble metal-based electrocatalysis,[90,91] and some have also reported using PEC reactions, which will be introduced.

Lin et al. reported nickel–phosphorous nanospheres (nanoNi–P) prepared by facile electrosynthesis that was efficient in hydrogen generation and reforming PET.[92] By examining the electrochemical characteristics of the activity of the nanoNi-P electrode, the oxidation of EG was found to be involved in the electrochemical formation of active NiOOH species. Higher amounts of active NiOOH sites led to increased activity for EG oxidation, and P played an important role in reserving the active NiOOH species. Electrocatalytic EG oxidation on a nanoNi-P electrode

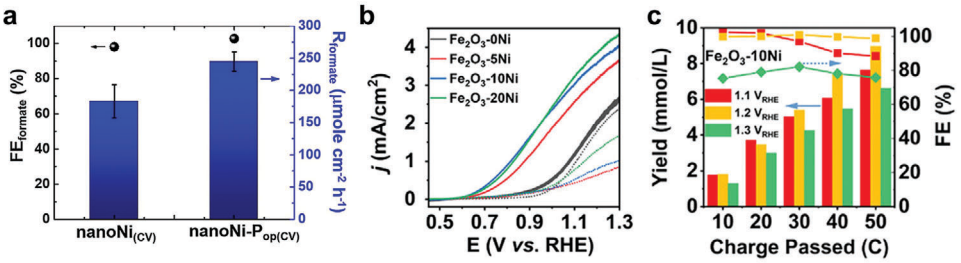

Figure 4. a) The production rate of formate ($R_{formate}$) and corresponding $FE_{formate}$ at nanoNi$_{(CV)}$ and nanoNi-P$_{op(CV)}$ from CPE. CPEs were performed at 1.5 V versus RHE in the deaerated KOH solution (1.0 M) containing EG (0.1 M). Reproduced with permission.[92] Copyright 2021, Elsevier. b) LSV curves of the Fe_2O_3-*x*Ni ($x = 0$, 5, 10, and 20) photoelectrodes. The data were collected in 1 M KOH solution with (solid lines) and without (dash-dotted lines) the presence of 50×10^{-3} M PET hydrolysate. c) Concentration of the generated formic acid and the corresponding FE of Fe_2O_3–10Ni at different applied biases of 1.1, 1.2, and 1.3 V versus RHE. Reproduced with permission.[93] Copyright 2022, American Chemical Society.

prepared in the presence of hypophosphite after cyclic voltammetry (CV) activation (nanoNi–P$_{op(CV)}$) generated formate as a product with nearly 100% FE (**Figure 4**a). The nanoNi–P electrode was further integrated onto a TiO_2 nanorod (nanoTiO_2) photoanode to explore the characteristics of PEC EG oxidation. The photocurrent response of nanoTiO_2|nanoNi–P was approximately five times higher than that of bare nanoTiO_2 at a potential of 0.4 V versus RHE and exhibited a lower photocurrent onset potential by approximately 200 mV. As a result, the formic acid yield of nanoTiO_2|nanoNi–P was 2.1 μmol cm^{-2} h^{-1} with an FE of 57.2% at 0.5 V versus RHE, whereas the bare nanoTiO_2 showed only 0.3 μmol cm^{-2} h^{-1} formic acid yield with an FE of 27.0%. The relatively low FE of PEC EG oxidation compared to EC EG oxidation occurred because the small loading amount of nanoNi–P on nanoTiO_2 could not fully cover nanoTiO_2, thus revealing the bare nanoTiO_2 surface to EG.

Li et al. proposed a new working mechanism for the selective oxidation of EG to formic acid on an Fe_2O_3/Ni(OH)$_x$ photoanode.[93] The Ni(OH)$_x$ cocatalyst was capable of efficiently converting EG into desired chemicals and modulating the oxidation abilities of the photogenerated holes to prevent overoxidation into valueless CO_2. The Ni(OH)$_x$ cocatalyst was loaded on the Fe_2O_3 photoanode by a facile hydrothermal treatment, in which the samples were named Fe_2O_3-*x*Ni ($x = 0$, 5, 10, and 20) depending on the Ni^{2+} concentrations of the precursor, and the PEC performances were evaluated in a 1 M KOH electrolyte in the presence and absence of 50×10^{-3} M PET hydrolysate. The photoanode with Ni(OH)$_x$ cocatalysts exhibited critically enhanced photocurrent density with an ≈300 mV lowered onset potential in the presence of PET hydrolysate in the electrolyte (Figure 4b), whereas the PEC performance of the bare Fe_2O_3 photoanode showed little difference with the introduction of the PET hydrolysate; thus, the key factor for the PEC oxidation of EG was the Ni(OH)$_x$ cocatalyst. The Fe_2O_3 photoanode with an adequate decorated amount of Ni(OH)$_x$ cocatalysts showed an FE of nearly 100% for formic acid at 1.2 V versus RHE. Additionally, similar PEC performances in different concentrations of PET hydrolysate demonstrated that the Fe_2O_3/Ni(OH)$_x$ photoanodes are promising for PEC catalysis of PET waste plastics. Based on the results, researchers proposed that the Ni^{2+}/Ni^{3+} redox couple is responsible for the selective oxidation of PET hydrolysate. Ni^{2+} species were oxidized by the photogenerated holes from the Fe_2O_3 photoanode to the higher valence of Ni^{3+} and were reduced back to the Ni^{2+} state after oxidation of EG into formic acid. This was different in the conventional PEC water oxidation reaction, in which Ni^{2+} species are continuously oxidized into Ni^{3+} to provide active sites for the reactions to take place. Therefore, the Ni(OH)$_x$ cocatalyst effectively modulated the oxidation ability of the photogenerated holes to stop EG from further overoxidizing into CO_2 and exhibited high selectivity toward formic acid. Recently, the same group integrated the Fe_2O_3/Ni(OH)$_x$ photoanode with an ultrathin TiO_x interlayer to increase the photocurrent density by improving the photogenerated charge carrier kinetics and to exhibit long-term stability for upcycling PET plastic wastes.[94] The optimal photoanode achieved an average formic acid yield of 0.277 mol m^{-2} h^{-1} and maintained a high FE of 95% toward formic acid with a negligible amount of glycolic acid intermediate produced (Figure 4c).

3.1.4. Glycerol

Glycerol, a main byproduct of biodiesel, has gained attention due to the favorable applications of its oxygenated compounds, such as aldehydes, ketones, and carboxylates.[95–97] Owing to its three hydroxyl groups, glycerol can be oxidized into many different valuable products, such as 1,3-dihydroxyacetone (DHA), glyceraldehyde (GLD), and formic acid. DHA is widely used in the pharmaceutical, fine chemical, cosmetic, and food industries, and commercially, DHA is mainly produced by microbial fermentation processes.[98–100] On the other hand, GLD is an industrially important chemical that is used in the preparation of adhesives and polyesters and is also used in the pharmaceutical industry to synthesize antibiotics and anticancer drugs.[101] Accordingly, the main two products with the highest value are DHA and GLD, which have market prices of 150 USD kg^{-1} and ≈40 USD kg^{-1}, respectively, whereas the market prices for crude and refined glycerol are only 0.11 USD kg^{-1} and 0.66 USD kg^{-1}, respectively.[102–105] Thus, oxidizing glycerol into DHA is desired in economics, but it is challenging to acquire both selectivity and kinetics; therefore, selective oxidation toward certain products other than DHA is equally important. Some papers on the PEC glycerol oxidation for the production of value-added chemicals are summarized in **Table 1**.

PEC oxidation of glycerol results in the production of DHA and GLD depending on which hydroxyl group of glycerol participates in the oxidation process. Oxidation of the middle hydroxyl

Table 1. List of value-added chemicals produced by PEC glycerol oxidation.

Catalyst	Light condition	Potential	Electrolyte	Main product	Selectivity [%]	Photocurrent [mA cm^{-2}]	Refs.
Bi_2WO_6	120 mW cm^{-2} ($\lambda > 350$ nm)	1.3 V vs RHE	0.1 M K_2SO_4 10 v % glycerol (pH 4)	FA	88[a)]	0.29	[106]
Ta_2N_5/CoNiFe-LDH	AM 1.5 G (100 mW cm^{-2})	1.23 V vs RHE	1.0 M NaOH 10 v % glycerol (pH 13.6)	FA	≈100%	3.59	[108]
$BiVO_4$	AM 1.5 G (100 mW cm^{-2})	1.2 V vs RHE	0.5 M Na_2SO_4 0.1 M glycerol (pH 2)	DHA	51	3.7	[109]
$BiVO_4$	AM 1.5 G (100 mW cm^{-2})	1.1 vs RHE	0.1 M NaBi 0.1 M glycerol (pH 2)	DHA	60	1.4	[115]
$BiVO_4$	AM 1.5 G (100 mW cm^{-2})	1.23 vs RHE	0.5 M Na_2SO_4 0.1 M glycerol (pH 2)	DHA	53.7	6.04	[121]
$BiVO_4$/NiCo-LDH-Act	AM 1.5 G (100 mW cm^{-2})	1.4 vs RHE	0.5 M Na_2SO_4 0.6 M glycerol (pH 7)	DHA	41.93	5.5[b)]	[114]
Bi_2O_3/TiO_2	AM 1.5 G (100 mW cm^{-2})	1.0 vs RHE	0.5 M Na_2SO_4 0.1 M glycerol (pH 2)	DHA	75.4	2.3[b)]	[112]
TiO_2(N-C)/CPB/TiO_2	–	1.2 vs RHE	0.1 M Na_2SO_4 10 v% glycerol (pH 2)	DHA	51[b)]	4.5	[113]
TiO_2/LDH/Ag	AM 1.5 G (100 mW cm^{-2})	1.2 vs RHE	0.5 M Na_2SO_4 0.1 M glycerol (pH 7)	DHA	72.1	2.12	[118]
p-C_3N_4/Au	AM 1.5 G (100 mW cm^{-2})	1.0 vs RHE	1.0 M KOH 1.0 M glycerol	DHA	53.7	19[b)]	[111]
WO_3	AM 1.5 G (100 mW cm^{-2})	1.2 vs RHE	0.1 M Na_2SO_4 1 M glycerol (pH 2)	GLD	80	3.5	[116]
WO_3	LED UV lamp (350 mW cm^{-2})	0.6 vs Ag/AgCl (KCl Sat.)	0.5 M Na_2SO_4 0.1 M glycerol (pH 5.5)	GLD	65[b)]	0.3[b)]	[119]
WO_3/TiO_2	AM 1.5 G (100 mW cm^{-2})	1.2 vs RHE	0.5 M Na_2SO_4 0.1 M glycerol 0.1 M borate buffer (pH 6)	GLD	62[b)]	2.8[b)]	[120]

[a)] C-based selectivity; [b)] Approximately estimated.

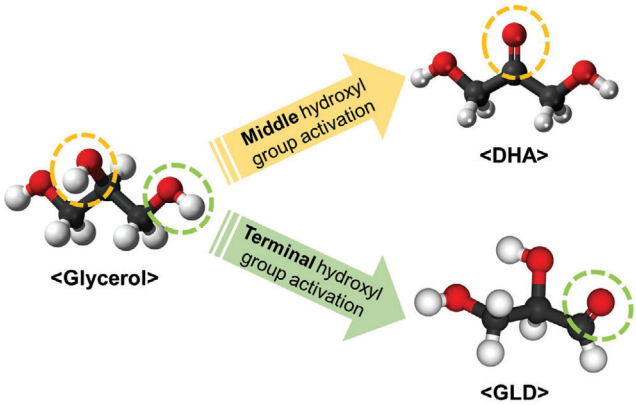

Figure 5. Schematic illustration of two different glycerol oxidation reaction pathways depending on which hydroxyl group is activated.

group results in the formation of DHA, whereas the oxidation of the terminal hydroxyl group results in the formation of GLD (**Figure 5**).

Further oxidation of DHA or GLD is known to produce formic acid as a liquid product and CO_2 as a gas product. As mentioned in the previous sections, formic acid is also a valuable product; therefore, researchers have also reported glycerol oxidation to formic acid with high selectivity and FE. Nascimento et al. evaluated the PEC reforming of glycerol aqueous solutions with Bi_2WO_6 photoanodes under different pH conditions.[106] Recent studies have shown that Bi_2WO_6 photocatalysts can selectively convert glycerol into DHA, triggering the desire to broaden the use of Bi_2WO_6 photocatalysts in PEC cells to overcome the disadvantages of photocatalysis, such as low reaction rates and low quantum efficiencies.[107] However, glycerol and its oxidation products remained strongly adsorbed on the Bi_2WO_6 surface, showing poor desorption and leading to a high selectivity of formic acid. The highest selectivity to formic acid (88%) was found in the pH 4 electrolyte with an initial glycerol concentration of 10% v/v under 1.30 V versus RHE with 120 mW cm^{-2} irradiation. Wang et al. modified 1D Ta_3N_5 nanoarrays with 2D trimetallic CoNiFe-LDH nanosheets as a novel integrated photoanode and examined its PEC glycerol oxidation properties.[108] The integration of trimetallic CoNiFe-LDH nanosheets featured increased specific surface active sites, promoted hole extraction, and improved charge separation efficiency. Nearly 100% FE for formate production was achieved in the first 30 minutes, which slowly decreased to 60% after 120 min due to the partial oxidation of formate and the competitive water oxidation reaction.

To gain high selectivity toward other valuable products, DHA and GLD, researchers have tried to engineer electrodes to prevent overoxidation to formic acid or CO_2. Liu et al. synthesized porous $BiVO_4$ nanoarrays for the selective oxidation of glycerol to DHA with a selectivity of 51% in acidic media accompanied by other products such as formic acid and glyceric acid.[109] Theoretical calculations suggested that the high selectivity of DHA occurred because the adsorption of the hydroxyl group on the middle carbon was more stable than that on the terminal carbon (**Figure 6**a). Furthermore, an acidic environment also helped suppress the reaction toward acid products, preventing the consumption of DHA and the production of formic acid.[110]

Cocatalysts that are beneficial to the selectivity to middle hydroxyl oxidation were often integrated or doped onto photoanodes to improve DHA selectivity. Sun et al. synthesized Au nanoparticles supported by polymeric carbon nitride (p-C_3N_4) nanosheets for selective PEC oxidation of glycerol to DHA.[111] Here, Au exhibited moderate affinity for the middle hydroxyl group of glycerol, which favors selectivity toward DHA. Moreover, Au is a material with an outstanding localized surface plasmon resonance effect, showing enhanced PEC kinetics. The p-C_3N_4 semiconductor with a 2D morphology effectively generated electron–hole pairs owing to its unique electronic structure. As a result, integrating Au on p-C_3N_4 provided a high turnover frequency (TOF) value toward DHA of 4617 h^{-1} with a DHA selectivity of 53.7% at 1.0 V versus RHE. The adsorption energies of the middle and terminal hydroxyl groups on the Au/p-C_3N_4 photoanode were calculated to be −1.42 eV and −1.27 eV, respectively, indicating that Au showed an affinity for adsorption on the middle hydroxyl group, supporting the high DHA selectivity. Luo et al. prepared Bi_2O_3 nanoparticles supported on TiO_2 nanorod arrays (Bi_2O_3/TiO_2) for PEC glycerol oxidation to DHA with high selectivity.[112] Experimental data combined with theoretical studies showed that Bi_2O_3 preferred to interact with the middle hydroxyl group of glycerol to facilitate the selective oxidation of glycerol to DHA. Cooperating Bi_2O_3 with TiO_2 enhanced the optical absorption, and the formed p–n junction promoted charge transfer, resulting in improved photocurrent density. The Bi_2O_3/TiO_2 photoanode exhibited excellent DHA selectivity of 75.4% at 1.0 V versus RHE compared with the pristine TiO_2 photoanode, which showed a lower DHA selectivity of 22.3% (Figure 6b).

In an effort to improve the production rates of PEC glycerol oxidation, Tang et al. constructed a photoanode based on metal-organic framework-derived N-doped carbon TiO_2/$CsPbBr_3$/TiO_2 nanorods (MOF-derived TiO_2(N-C)/CPB/TiO_2 NRs).[113] The N-doped carbon (N-C) layer was regarded as the carrier transport channel that enhanced the charge transfer property to the system, increasing the carrier separation capability. The photogenerated electrons within $CsPbBr_3$ and TiO_2 were easily transferred to the TiO_2 nanorods through the N-C layer (Figure 6c). The TiO_2(N-C)/CPB/TiO_2 NR photoanode showed a superior photocurrent density of 4.5 mA cm^{-2} at 1.2 V versus RHE in the presence of glycerol compared with that of the bare TiO_2 photoanode, which showed a photocurrent density lower than 1.5 mA cm^{-2}. Moreover, the main products of PEC glycerol oxidation were DHA and GLD, with the highest total production rate of ≈425 mmol m^{-2} h^{-1} at 0.8 V versus RHE. Miao et al. reported a surface active oxygen engineering method through activation of NiCo layered double hydroxide (NiCo-LDH-Act) to increase surface oxidation reactions.[114] The activation process significantly increased the lattice oxygen content, which was attributed to the dehydrogenation of the hydroxyl group to expose the active oxygen on the LDH surface (Figure 6d). By integrating NiCo-LDH-Act on $BiVO_4$, hole transfer was promoted at the semiconductor/cocatalyst interface, and the surface reaction kinetics were accelerated, reaching a maximum DHA selectivity of 41.93% and a production rate of 20.5 μmol cm^{-2} h^{-1} at 1.4 V versus RHE (Figure 6e).

Vo et al. studied the effects of different crystallographic facet dependence of PEC glycerol oxidation on a $BiVO_4$ photoanode (**Figure 7**a).[115] The product yield for {010}-dominated $BiVO_4$ ({010}-BVO) was twofold greater than the amount obtained for

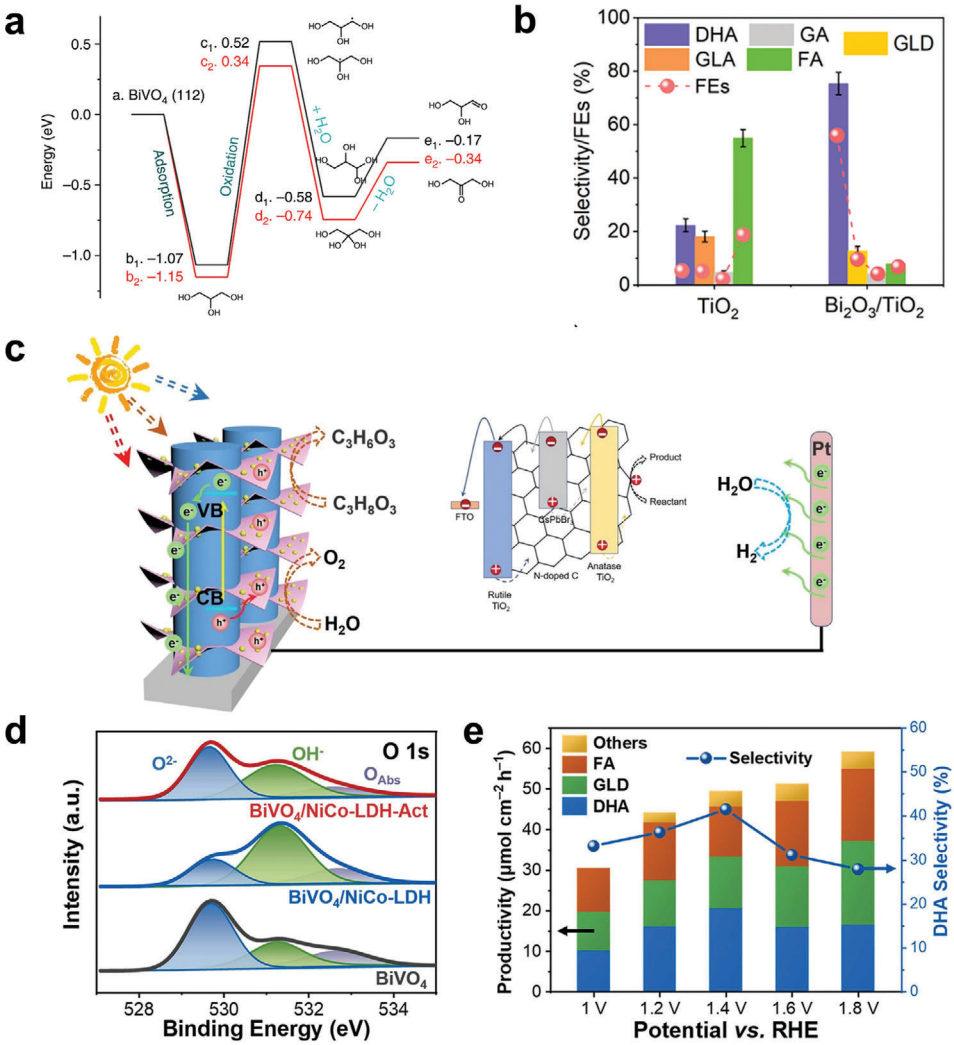

Figure 6. a) Energy profile of glycerol oxidation on $BiVO_4$. 1 (black) and 2 (red) represent reactions that take place at the terminal and middle carbon, respectively. Reproduced with permission.[109] Copyright 2019, Springer Nature. b) Selectivity and FE of organic products over TiO_2 and Bi_2O_3/TiO_2 photoanodes at 1.0 V versus RHE within 1 h. The organic products include DHA, GLD, glyceric acid (GLA), glycolic acid (GA), and formic acid (FA). Reproduced with permission.[112] Copyright 2022, American Chemical Society. c) Schematic illustration of the light-harvesting and carrier separation mechanism in the MOF-derived TiO_2(N-C)/CPB/TiO_2 NR photoanode. Reproduced with permission.[113] Copyright 2021, Elsevier. d) High-resolution XPS spectra of O 1 s for $BiVO_4$, $BiVO_4$/NiCo-LDH, and $BiVO_4$/NiCo-LDH-Act. e) Productivity of organic products and DHA selectivity over the $BiVO_4$/NiCo-LDH-Act photoanode at different potentials within 1 h. The products include DHA, GLD, formic acid, and others. Reproduced with permission.[114] Copyright 2023, Elsevier.

{121}-dominated $BiVO_4$ (r-BVO). {010}-BVO held a DHA selectivity of approximately 60%, which was slightly higher than that of r-BVO with a DHA selectivity of 45% (Figure 7b). The mechanistic study demonstrated that the middle hydroxyl group of glycerol could adsorb more on {010}-BVO than on r-BVO. Ouyang et al. also studied the effect of controlling the facet exposure on the selectivity for PEC glycerol oxidation with a WO_3 photoanode.[116] Upon illumination in the presence of glycerol, the photocurrent density of WO_3 with {202} facets (WO_3 {202}) reached 3.52 mA cm^{-2} at 1.23 V versus RHE, which was over 2 times higher than that of WO_3 with {200} facets (WO_3 {200}). Interestingly, the GLD production rate of WO_3 {202} (462 mmol m^{-2} h^{-1}) was 2.7 times higher than that of WO_3 {200}, with an outstanding GLD selectivity of 80% (Figure 7c). Theoretical calculations suggested that both photoanodes preferred the absorption of the terminal hydroxyl group of glycerol rather than the middle hydroxyl group, leading to the formation of GLDs (Figure 7d). Additionally, the lower barrier for the uphill product desorption on WO_3 {202} compared with WO_3 {200} supported the inhibition of overoxidation and higher GLD selectivity.

PEC glycerol oxidation is reported to occur predominantly via hydroxyl radicals, which show strong oxidation potentials to effectively oxidize glycerol.[117] However, overoxidation can occur, resulting in the production of lower value chemicals. Liu et al. explored the mechanism by which selective PEC glycerol oxidation occurs on Ag nanoparticle-supported layered double hydroxide sheets on TiO_2 (Ag@LDH@TiO_2) by mediating the oxidizing capability of surface-bound hydroxyl radicals.[118] The LDH

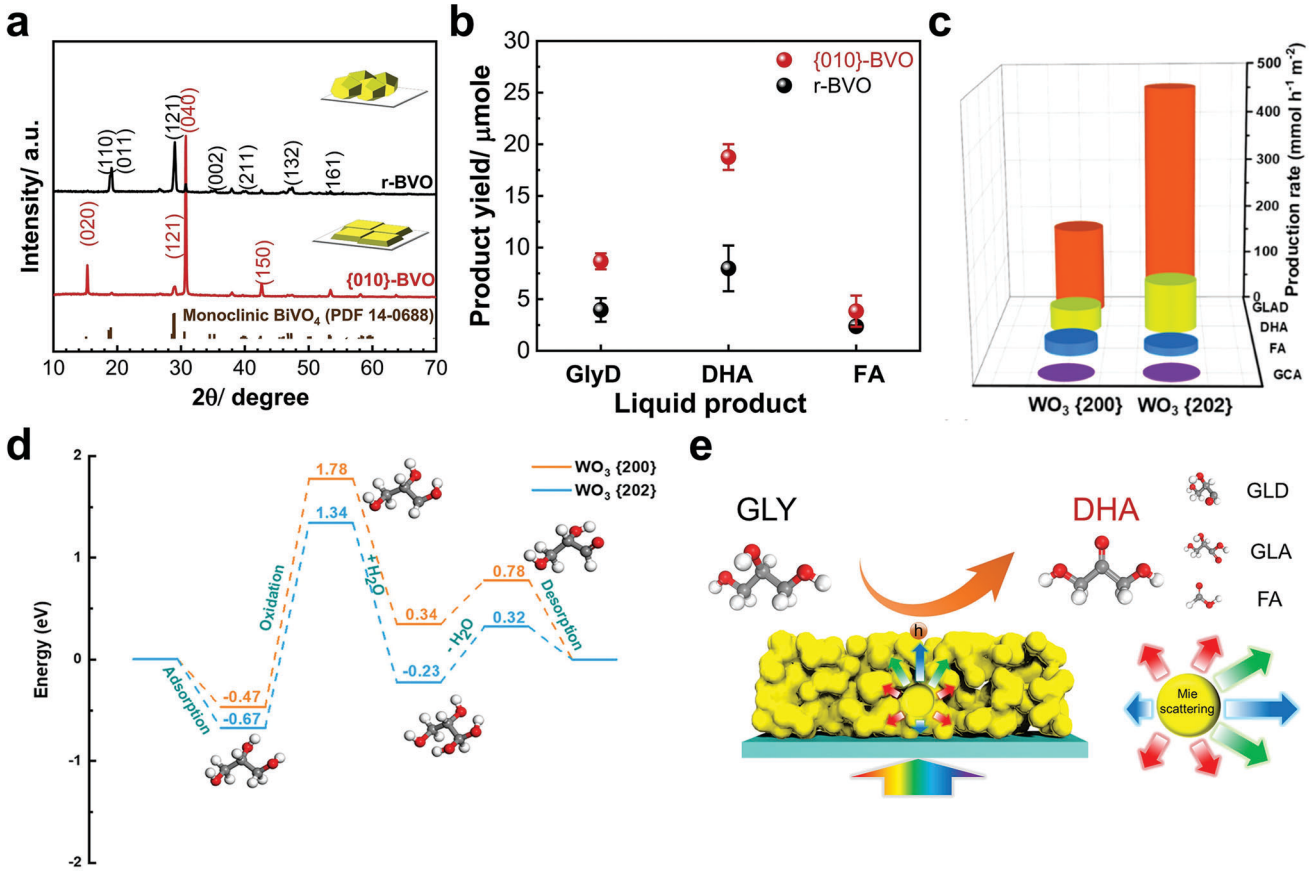

Figure 7. a) XRD pattern of r-BVO and {010}-BVO. b) Product concentration of the PEC glycerol oxidation reaction (GOR) over {010}-BVO and r-BVO after running the GOR for 2 h. Reproduced with permission.[115] Copyright 2020, Elsevier. c) Production rate of oxidation products over WO_3 {200} and WO_3 {202} photoanodes at 1.2 V versus RHE with 1 M glycerol (pH = 2). Products include glyceraldehyde (GLAD), DHA, formic acid (FA), and glycolic acid (GCA). d) Energy profiles of glycerol oxidation on WO_3 at {200} (orange) and {202} facets (blue). Reproduced with permission.[116] Copyright 2020, American Chemical Society. e) Schematic illustration of PEC glycerol oxidation to DHA using the MP-$BiVO_4$ photoanode. Reproduced with permission.[121] Copyright 2023, Wiley-VCH.

at the photoanode surface confined the surface-bound hydroxyl radicals by hydrogen-bonding interactions, exhibiting a DHA selectivity of 72% at 1.2 V versus RHE, which is higher than that of pure TiO_2 (23.5%). Yu et al. investigated the enhancement in the PEC glycerol oxidation ability and stability of a monoclinic WO_3 catalyst for the selective production of C_3 products, such as GLD and DHA.[119] Similar to previous research, hydroxyl radicals were expected to lead to more oxidized products, such as formic acid or CO_2. Here, the relatively higher PEC water oxidation activity shown by monoclinic WO_3 favored the consumption of adsorbed hydroxyl radicals for oxygen evolution, thus preventing overoxidation and increasing the selectivity toward C_3 products. The proposed monoclinic WO_3 exhibited a GLD selectivity of approximately 65% at 0.6 V versus Ag/AgCl, which was higher than that of the commercial WO_3/TiO_2 photoanode (49%).

Gu et al. constructed a microfluidic architecture with 3-D microflow channels constructed with WO_3/TiO_2 heterostructures on porous carbon fibers.[120] Due to the enhanced diffusion of glycerol molecules and their intermediates, the microfluidic platform not only exhibited high activity over a wide range of potentials (0.6–1.2 V versus RHE) but also inhibited the overoxidation of glycerol with a joint DHA/GLD selectivity of 85%. Recently, our group designed a porous $BiVO_4$ photoanode with an enhanced Mie scattering effect, which significantly reduced the reflectivity to near zero.[121] Mie scattering occurs when the particle size is close to the wavelength of the incident light. Therefore, $BiVO_4$ photoanodes were further treated to gain a large pore size of 512 nm, which is equivalent to the incident light. Due to the enhanced light absorbability by the Mie scattering effect (Figure 7e), the production rate of DHA by PEC glycerol oxidation was significantly improved to 325.2 mmol m^{-2} h^{-1}, which was nearly twofold higher than that of bare $BiVO_4$ (186.3 mmol m^{-2} h^{-1}). The high selectivity toward DHA (53.7%) was ascribed to the easier adsorption of the middle hydroxyl group of glycerol caused by strong electrostatic attraction between Bi^{3+} and the oxygen of the hydroxyl group.

Although most of the works reported DHA, GLD, and formic acid as the main products for PEC glycerol oxidation, some reported other chemicals as their main products. Lee et al. fabricated a cobalt-doped ZnO photoanode for selective PEC glycerol oxidation to glyceric acid.[122] The introduction of cobalt improved the photocatalytic ability by enhancing the accessibility of

glycerol to the surface with a photocurrent density of 0.51 mA cm^{-2} at 1.1 V versus RHE, which was significantly higher than that of the bare ZnO film (0.19 mA cm^{-2}) and produced glyceric acid as the main product. Wu et al. introduced a tungsten-doped $BiVO_4$ electrode combined with a nickel (oxy)hydroxide cocatalyst for the PEC oxidation of glycerol.[123] By oxidizing glycerol in a mild alkaline media (pH = 9.3), glycolaldehyde was observed for the first time in PEC glycerol oxidation, which was proposed to form from isomeric DHA/GLD species through C–C bond cleavage with a release of one equivalent amount of formic acid.

3.1.5. Benzyl Alcohol

Benzyl alcohol is an organic compound that consists of a primary alcohol with an aromatic ring and is easily found in natural sources, such as plants, fruits, and biomass. Although it contains an aromatic ring, benzyl alcohol is a polar molecule that can be dissolved easily in water. In terms of the PEC process, benzyl alcohol can be oxidized at the photoanode to produce benzaldehyde or benzoic acid, as shown in **Table 2**. Moreover, various derivatives of benzyl alcohol can be upgraded by a similar oxidation process at the photoanode, such as 4-methylbenzyl alcohol, 4-fluorobenzyl alcohol, and 4-chloro-1-phenyl-1-propanol. PEC oxidation of benzyl alcohol is among the challenges that must be solved for organic upgrading of chemicals that have aromatic rings, which may be applicable for various purposes, such as pharmaceutical manufacture and plastic production.

Light-driven benzyl alcohol oxidation was first reported by Markham et al. in 1958. They reported the photocatalytic oxidation of benzyl alcohol by using ZnO as a photocatalyst, and they suggested the possible production of benzaldehyde.[124] After that, photocatalytic benzyl alcohol oxidation was reported several times, while PEC benzyl alcohol oxidation was reported for the first time in 2014 by Song et al.[125] They prepared a dye-sensitized photoelectrosynthesis cell (DSPEC) consisting of a Ru-based dye coated on the surface of a nanoITO/TiO_2 core/shell structure (**Figure 8**a). The working principle of the dye-sensitized photoanode demonstrated that coloading of ruthenium polypyridyl chromophore and $[Ru(Mebimpy)((4,4'\text{-}(OH)_2PO\text{-}CH)_2bpy)\text{-}(OH_2)]^{2+}$ catalyst enabled active catalytic species of $[Ru(Mebimpy)((4,4'\text{-}(OH)_2PO\text{-}CH_2)_2bpy)\text{-}(O)]^{2+}$, while the optimized condition of DSPEC showed 37.1% FE and a sustained absorbed photon to current efficiency (APCE) of 3.7% for benzyl alcohol dehydrogenation. Similar to Song's work, Bai et al. reported PEC benzyl alcohol oxidation with a Ru catalyst-decorated hematite photoanode.[126] The PEC performance of the optimized photoanode showed remarkable enhancement in both onset potential and photocurrent density after decoration with the dye. Performance enhancement was observed again when benzyl alcohol was added to the electrolyte. The photoanode achieved 82% FE with a 31.6% yield of benzaldehyde production with the optimized Ru catalyst.

The reaction mechanism of PEC benzyl alcohol oxidation was proposed in some papers.[127,128] Zhou et al. reported selective PEC benzyl alcohol oxidation by using a Bi_2MoO_6@TiO_2NTA photoanode.[127] It was found that the Lewis acid site of Mo atoms in Bi_2MoO_6 can efficiently adsorb benzyl alcohol, which contains a lone pair of electrons in the hydroxyl group and then oxidizes benzyl alcohol to an active anion ($*C_6H_5\text{–}CH_2OH^+$), as presented in Figure 8b. Furthermore, nearby Lewis base sites in Bi_2MoO_6 adsorb $\bullet O_2^-$ radicals, which finally oxidize $*C_6H_5\text{–}CH_2OH^+$ into benzaldehyde. As mentioned by Zhou et al., the Lewis base of the hydroxyl group in benzyl alcohol provides lone pair electrons that enable adsorption on the catalytic surface. This was of interest because most aromatic compounds are difficult to apply in electrochemical systems because they are nonpolar and they cannot easily adsorb on the catalyst surface. Luo et al. reported PEC benzyl alcohol oxidation by using bismuth vanadate (BVO) decorated with ultrathin layered double hydroxide (U-LDH) and graphene (G), namely, G@U-LDH@BVO.[128] They compared two cocatalyst materials, U-LDH and Co_3O_4, for benzyl alcohol oxidation. Interestingly, G@U-LDH@BVO showed continuous benzaldehyde selectivity over 60 C of charge passed, while G@Co_3O_4@BVO showed degradation of selectivity after some time. Thus, Fourier transform infrared spectroscopy (FT-IR) was carried out to investigate the chemicals adsorbed on the Co_3O_4 and U-LDH surfaces. They found that the FT-IR spectra of Co_3O_4 showed C=O and –CHO bonding at 1684 cm^{-1} and 1204 cm^{-1}, respectively, while no peaks appeared in U-LDH, demonstrating that Co_3O_4 suffers from slow desorption of intermediates formed during the oxidation reaction from benzyl alcohol to benzaldehyde, while U-LDH exhibited superior desorption properties to enable high stability over time (Figure 8c). By combining the results of electron spin resonance (ESR), isotope labeling experiments, and FT-IR, the researchers proposed the reaction mechanism of benzyl alcohol oxidation to benzaldehyde on the catalyst surface. As shown in Figure 8d, the hydroxyl group of benzyl alcohol is first adsorbed on the LDH surface, followed by conversion into carbon-centered radicals. After that, •OH radicals generated from the water activated the C–O bond to finally produce benzaldehyde.

The hydroxyl group of benzyl alcohol allows water solubility and adsorption on the catalyst surface, which facilitate PEC oxidation to aldehyde, while the aromatic part of benzyl alcohol is less conjugated in the PEC reaction. Paradoxically, due to the lower influence of the aromatic part on the PEC reaction, its simple derivatives are readily oxidized into aldehydes.[127,129,130] Various kinds of benzyl alcohol derivatives that are capable of being used as substrate materials for PEC reactions are shown in Figure 8e. For instance, Zhang et al. reported the PEC oxidation of several aromatic alcohols over a TiO_2/C photoanode.[129] Aromatic alcohols, such as benzyl alcohol, 4-methylbenzyl alcohol, 4-fluorobenzyl alcohol, and 1-phenyl-1-propanol, showed 100% aldehyde selectivity, but the production of 1-phenyl-1-propanol was relatively lower than that of the others. The researchers suggested that the steric hindrance of the propanol group in 1-phenyl-1-propanol compared to the ethanol group in benzyl alcohol may affect the oxidation on the photoanode surface. On the other hand, 4-methylbenzyl alcohol oxidation showed the highest production of aldehyde compared to that of the others. A similar result of high production of 4-methylbenzyl aldehyde was again observed by Luo et al.[128] Here, 4-fluorobenzyl alcohol, 4-chlorobenzyl alcohol, 4-bromobenzyl alcohol and 4-methylbenzyl alcohol were used as substrate materials. All substrate reactions showed nearly similar results for the conversion, selectivity, and yield compared with benzyl alcohol oxidation, while one remarkable result is in the case of 4-methylbenzyl alcohol oxidation, in

Table 2. List of value-added chemicals produced by PEC benzyl alcohol oxidation.

Catalyst	Light condition	Potential	Electrolyte	Main product	Selectivity [%]	Photocurrent [mA cm^{-2}]	Refs.
NanoITO /TiO_2 with $Ru^{II}P^{2+}$ and $Ru^{II}OH_2^{2+}$	λmax = 445 nm, fwhm ≈20 nm, ≈1.7–83 mW	0.2 V vs NHE	0.1 M benzyl alcohol in 20×10^{-3} M pH 4.5 acetate/acetic acid buffer with 0.1 M $LiClO_4$	Benzaldehyde	66[a)]	0.029[b)]	[125]
α-Fe_2O_3	AM 1.5G (100 mW cm^{-2})	1.0 V vs RHE	0.02 M benzyl alcohol in 0.05 M potassium hydrogen phthalate and 0.45 M $LiClO_4$	Benzaldehyde	88[a)]	0.18	[126]
Bi_2MoO_6@TiO_2NTA	AM 1.5G (100 mW cm^{-2})	–	0.1 M benzyl alcohol in 0.1 M Na_2SO_4	Benzaldehyde	98.6	0.58	[127]
G@U-LDH @BVO	AM 1.5G (100 mW cm^{-2})	1.2 V vs RHE	2 mmol benzyl alcohol in 10 mL of 0.1 M PBS	Benzaldehyde	99	3.0	[128]
TiO_2/C /Co_3O_4	120 mW cm^{-2}	–	1 mL benzyl alcohol in 0.5 M Na_2SO_4	Benzaldehyde	100	–	[129]
Carbon nitride	AM 1.5G (100 mW cm^{-2})	1.22 V vs RHE	10×10^{-3} M benzyl alcohol in 1.0 M NaOH	Benzaldehyde	99	0.62	[130]
Poly(perylenecarboxylate) thin films	Blue LED bulb (3 W)	0.6 V vs Ag/AgCl (KCl Sat.)	40×10^{-3} M benzyl alcohol in 0.1 M $TBAFP_6$ with 2×10^{-3} M TEMPO	Benzaldehyde	–	0.018	[131]
$BiVO_4$	AM 1.5G (100 mW cm^{-2})	0.6 V vs SCE	25×10^{-3} M benzyl alcohol, 100×10^{-3} M pyridine, 0.1 M $TBAFP_6$ in acetonitrile with 5×10^{-3} M TEMPO	Benzaldehyde	85[a)]	0.425	[132]
hyd–ZnP + ac-TEMPO	100 mW cm^{-2} with 400 nm cutoff filter	–	50×10^{-3} M benzyl alcohol, 100×10^{-3} M pyridine, 0.1 M $TBAFP_6$ in acetonitrile with 5×10^{-3} M TEMPO	Benzaldehyde	82[a)]	0.2	[133]
Thienopyrroledione-based dye sensitized TiO_2/S-TEMPO	50 mW cm^{-2} LED lamp	0 V vs Ag/AgCl (KCl Sat.)	1.2 M LiTFSI, 1.0 MTEMPO, 0.1 M benzyl alcohol, 0.2 M C_6H_5Cl in 3 mL acetonitrile	Benzaldehyde	100[a)]	–	[134]
Thienopyrroledione-based dye-sensitized TiO_2	50 mW cm^{-2} LED lamp	0 V vs Ag/AgCl (KCl Sat.)	1.2 M LiTFSI, 1.0 MTEMPO, 0.1 M benzyl alcohol, 0.2 M C_6H_5Cl in 3 mL acetonitrile	Benzaldehyde	100[a)]	0.4	[135]

[a)] Faradaic efficiency; [b)] Approximately estimated.

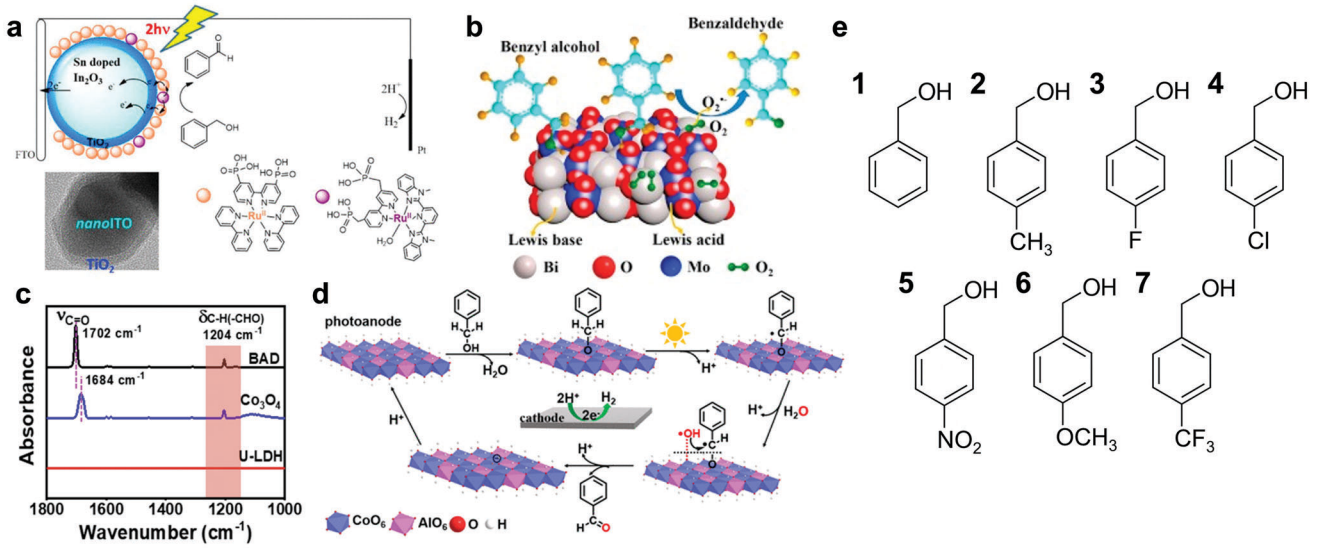

Figure 8. a) Schematic illustration of a dye-sensitized photoelectrosynthesis cell consisting of a Ru-based dye and catalyst. Reproduced with permission.[125] Copyright 2014, American Chemical Society. b) PEC benzyl alcohol oxidation mechanism on the Bi_2MoO_6@TiO_2NTA photoanode surface. The adsorption of benzyl alcohol and $\bullet O_2^-$ radicals at Lewis acid and base sites, respectively, is presented. Reproduced with permission.[127] Copyright 2021, Elsevier. c) FT-IR results demonstrating adsorbed benzaldehyde species on Co_3O_4 and U-LDH after reaction. d) Oxidation mechanism of benzyl alcohol to benzaldehyde on the G@U-LDH@BVO photoanode. Reproduced with permission.[128] Copyright 2020, American Chemical Society. e) Chemical structures of various kinds of benzyl alcohol derivatives. (1) Benzyl alcohol, (2) 4-methylbenzyl alcohol, (3) 4-fluorobenzyl alcohol, (4) 4-chlorobenzyl alcohol, (5) 4-nitrobenzyl alcohol, (6) 4-methoxybenzyl alcohol, (7) 4-(trifluoromethyl)benzyl alcohol.

which its conversion and yield are slightly larger than that of the others. They demonstrated that the electron-donating groups rather than electron-withdrawing groups favored the reactivity of aromatic alcohols, which resulted in higher production of 4-methylbenzyl aldehyde than that of the others.

Recently, among various kinds of organocatalysts, (2,2,6,6-tetramethylpiperidin-1-yl)oxyl, namely, TEMPO, has drawn attention because of its attractive catalytic property, in which TEMPO can selectively oxidize alcohol into aldehyde. The special selectivity of TEMPO originates from its stable aminoxyl radical, while the stability of this aminoxyl radical is secured by the surrounding four methyl groups providing steric protection. TEMPO-driven alcohol-to-aldehyde oxidation occurs in a catalytic cycle(**Figure 9**a). Briefly, the aminoxyl group in TEMPO is converted to an oxoammonium group by an oxidant. Then, the adjacent alcohol releases the proton in the hydroxyl group, while the oxygen bonds with the nitrogen at the oxoammonium group. Furthermore, the oxygen at the oxoammonium group takes the proton from the alcohol group, thereby producing an aldehyde. Then, the remaining hydroxylamine group is converted to an oxoammonium group by an oxidant again. The oxidant for the catalytic cycle of TEMPO can be alternated by the hole transferred from the light-absorbed photoanode in PEC cells, and this is how the PEC TEMPO system converts alcohol to aldehyde.

Zhuang et al. reported PEC benzyl alcohol by using a poly(perylenecarboxylate) (PPCA) thin film photoanode with TEMPO in the electrolyte.[131] The PPCA photoanode showed a relatively low photocurrent density of 5.36 μA cm^{-2} at 0.6 V versus Ag/AgCl, while the addition of TEMPO to the electrolyte helped increase the photocurrent density up to 18.35 μA cm^{-2} at the same potential (Figure 9b). The researchers suggested that the photogenerated holes in the PPCA thin film moved to the surface and oxidized the TEMPO radicals into oxoammonium intermediates. After that, the generated oxoammonium intermediates finally oxidized benzyl alcohol to benzaldehyde (Figure 9c). McMillan et al. developed a $BiVO_4$ photoanode for TEMPO-mediated benzyl alcohol oxidation, and a schematic illustration of the system is presented in Figure 9d.[132] $BiVO_4$ is a well-known n-type PEC material with favorable band alignment and light absorption properties over the visible light region. Owing to its properties, the photocurrent density reached 0.28 mA cm^{-2} at 0.3 V versus SCE, and the FE for benzaldehyde formation was approximately 85%. More interestingly, the addition of pyridine into the electrolyte significantly increased the FE from 44% to 85% (Figure 9e). Pyridine is known as a hole transfer molecule applied in organic photovoltaics and perovskite solar cells. In this paper, pyridine may transfer holes from the $BiVO_4$ surface to TEMPO while reducing unwanted hole consumption at the $BiVO_4$ surface, resulting in increased selectivity for benzyl alcohol oxidation.

To improve the light absorption property of TEMPO-assisted photoanodes, the dye sensitization method has been applied recently.[133–135] Most dyes are not stable in aqueous media, especially for dye-sensitized photoanodes, which is the first hurdle that must be overcome. Therefore, most dye-sensitized TEMPO-assisted PEC cells were developed in organic electrolytes such as acetonitrile. Nikoloudakis et al. reported a zinc porphyrin sensitizer-decorated TiO_2 photoanode for DSPEC benzyl alcohol oxidation.[133] They compared the PEC benzyl alcohol oxidation performance in both aqueous and organic electrolytes. In an aqueous electrolyte, the leaching of the photocatalyst from the TiO_2 electrode was the main activity that hindered the photoanode's performance. In the organic electrolyte, porphyrin dye degradation was the major cause of photoanode degradation.

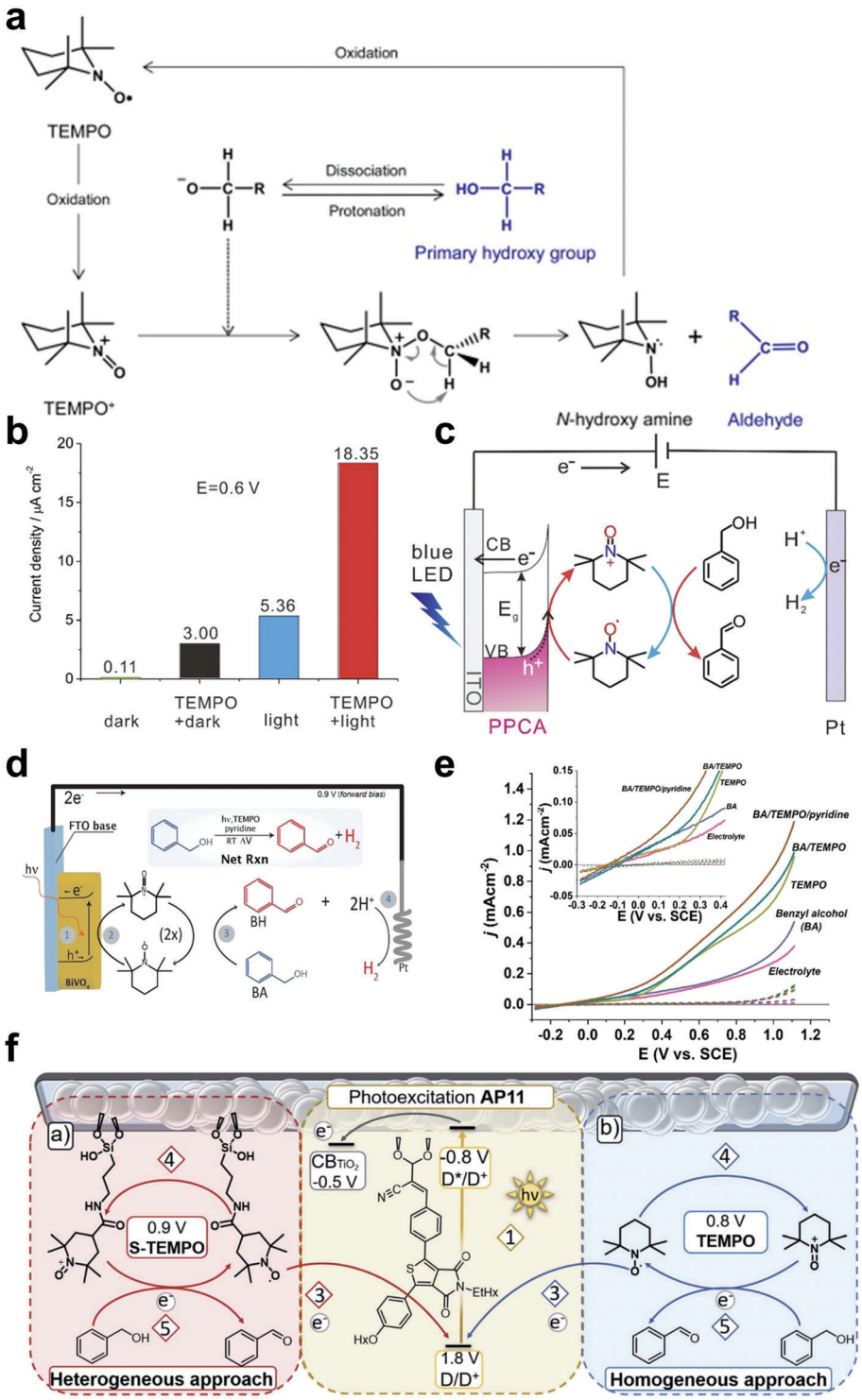

Figure 9. a) Reaction mechanism of TEMPO-assisted alcohol to aldehyde oxidation. Reproduced with permission.[136] Copyright 2018, Elsevier. b) Comparison graph of photocurrent density at 0.6 V generated from benzyl alcohol oxidation using the PPCA photoanode. c) Schematic illustration of TEMPO-mediated PEC benzyl alcohol oxidation using a PPCA photoanode. Reproduced with permission.[131] Copyright 2020, American Chemical Society. d) Schematic illustration of TEMPO-mediated PEC benzyl alcohol to benzaldehyde oxidation using $BiVO_4$ and pyridine as a photoanode and redox mediator, respectively. e) *J–V* curve of the $BiVO_4$ photoanode. The PEC performance of $BiVO_4$ is the highest when TEMPO and pyridine are used for benzyl alcohol oxidation. Reproduced with permission.[132] Copyright 2022, Wiley-VCH. f) Schematic illustration of two different approaches of benzyl alcohol oxidation using TEMPO-assisted AP11 dye-sensitized PEC cells: a) heterogeneous approach, b) homogeneous approach. Reproduced with permission.[134] Copyright 2021, The Royal Society of Chemistry.

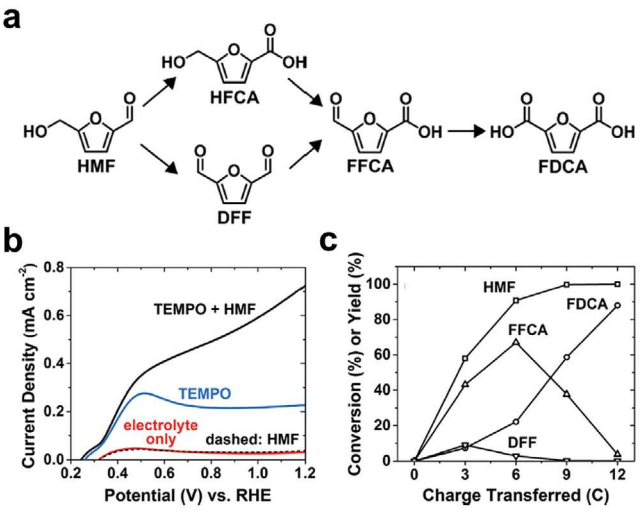

Figure 10. a) Reaction pathways for HMF oxidation to FDCA. b) LSV curves under AM1.5G illumination for $BiVO_4$/CoPi-30 under various electrolyte conditions. c) HMF conversion efficiency and product yields for $BiVO_4$/CoPi-30 photoelectrodes at 0.64 V versus RHE with illumination. Reproduced with permission.[141] Copyright 2019, Wiley-VCH.

Additionally, they found that anchoring TEMPO with zinc porphyrin makes recovery of the catalytic system much easier. With respect to anchoring TEMPO to the dye, Bruggeman et al. compared homogeneous and heterogeneous benzyl alcohol oxidation by PEC cells.[134] They used TiO_2 sensitized with thienopyrroledione-based dye AP11 as a photoanode and compared the PEC performance when TEMPO was immobilized to the dye with the performance when it was not immobilized (Figure 9f). Interestingly, the immobilization of TEMPO demonstrated an insufficient ability to mediate electron transfer from the substrate to the dye, which resulted in poor stability. In addition, a homogenous approach that enabled efficient electron transfer mediated through the substrate to the dye showed better light-driven benzyl alcohol oxidation performance and was stable over 32 h of operation.

3.2. Complex Hydrocarbons

3.2.1. 5-Hydroxymethylfurfural

5-hydroxymethylfurfural (HMF), which is obtained from the depolymerization of cellulosic biomasses, is regarded as a key intermediate that can undergo further conversion to generate industrially important and valuable compounds.[137] For example, following the reaction pathway in **Figure 10**a, HMF with a market price of 1.03 USD kg^{-1} can be oxidized to 2,5-furandicarboxylic acid (FDCA) with an extremely high market price of 306 USD/kg, which serves as a monomer to produce useful polymers such as polyethylene terephthalate, polyethylene furanoate, polypropylene furan-dicarboxylate, or polybutylene furan-dicarboxylate.[138,139] Conventionally, high temperature, high-pressure O_2, alkaline conditions (pH >13) and the use of precious-metal catalysts were needed, but after the pioneering work of Cha and Choi, it was found that PEC oxidation of HMF under ambient conditions resulted in its complete conversion to FDCA, which triggered research toward efficient PEC HMF oxidation.[140] And recent works on PEC HMF oxidation to produce value-added chemicals are summarized in **Table 3**.

As mentioned, Cha et al. were the first to demonstrate 6-electron PEC HMF oxidation to FDCA, as shown in Equation 15. Using $BiVO_4$ as the photoanode and TEMPO as a mediator, a low onset potential of 0.32 V versus RHE was achieved, and an almost complete conversion of HMF to FDCA was observed after 40 C of charge passed, with an FDCA FE of 93%. These results suggested that TEMPO-mediated HMF conversion is kinetically and thermodynamically more favorable than water oxidation. The simultaneous enhancement in value, efficiency, and utility of the anodic reaction suggested TEMPO-mediated HMF oxidation as a viable alternative to OER.

$$HMF + 6OH^- \rightarrow FDCA + 4H_2O + 6e^- \quad (15)$$

Chadderdon et al. applied cobalt phosphate (CoPi), a widely known OER cocatalyst, to a $BiVO_4$ photoanode.[141] Contrary to the presumable assumption that CoPi favorably promotes OER over TEMPO oxidation, Chadderdon et al. suggested that CoPi alleviates back reduction of oxidized TEMPO and the resulting recombination losses. As a result, the onset potential decreased and the photocurrent was enhanced, allowing the $BiVO_4$/CoPi photoanode to achieve an 88% yield of FDCA at 0.64 V versus RHE (Figure 10b,c).

Although TEMPO-mediated HMF oxidation is promising, the presence of TEMPO makes it challenging to separate the product and hinder visible light absorption of the photoanode via parasitic absorption. To overcome these drawbacks, Lhermitte et al. utilized a WO_3 photoanode to realize mediator-free direct PEC HMF oxidation.[142] Owing to the highly oxidizing valence band maximum (VBM) and poor OER selectivity of WO_3, the onset potential was reduced by 100 mV, and the photocurrent was increased by 26% to 1.52 mA cm^{-2} by a simple addition of HMF. After a long-term PEC operation of 64 h, 2,5-furandicarboxaldehyde (DFF) was the major product with a 4% yield, while the FDCA yield was limited to < 1%, showing that oxidation of hydroxyl groups is kinetically favorable on the WO_3 surface.

Despite the promising future of PEC HMF oxidation, their development remains in a beginning phase, and a fundamental knowledge of their reactive mechanism and the development of various strategies are still highly desired for efficient and stable operation.

3.2.2. Cyclohexane and Cyclohexene

Oxidation of cyclohexane is among the least efficient but most important reactions. Oxidation of C–H bonds in cyclohexane yields cyclohexanone (C-one, K) and cyclohexanol (C-ol, A), the mixture of which is known as KA oil. KA oil is an important intermediate chemical for manufacturing textiles, such as nylon-6 and nylon-6,6 polymers, and possesses a higher market price (2.165 USD kg^{-1}) compared to cyclohexane (1.093 USD kg^{-1}).[142–145] In fact, their production worldwide surpasses 200 kton per year, which highlights the importance of cyclohexane oxidation.[146] However, like many other hydrocarbons, the oxidation of cyclohexane requires the activation of stable C–H bonds, which is

Table 3. List of value-added chemicals produced by PEC HMF oxidation.

Catalyst	Light condition	Potential [V vs RHE]	Electrolyte	Main product	Selectivity [%]	Photocurrent [mA cm^{-2}]	Refs.
$BiVO_4$	AM 1.5G (100 mW cm^{-2})	1.04 V vs RHE	0.5 M borate 7.5×10^{-3} M TEMPO 5×10^{-3} M HMF (pH 9.2)	FDCA	72	–	[140]
CoPi/$BiVO_4$	AM 1.5G (100 mW cm^{-2})	0.64 V vs RHE	0.2 M sodium borate 5×10^{-3} M TEMPO 5×10^{-3} M HMF (pH 9.2)	FDCA	88	0.4[a)]	[141]
WO_3	AM 1.5G (100 mW cm^{-2})	0.68 V vs RHE	0.1 M NaPi 5×10^{-3} M HMF (pH 4)	DFF	4	0.3–0.1[a,b)]	[142]

[a)] Approximately estimated; [b)] Photocurrent was decayed over time.

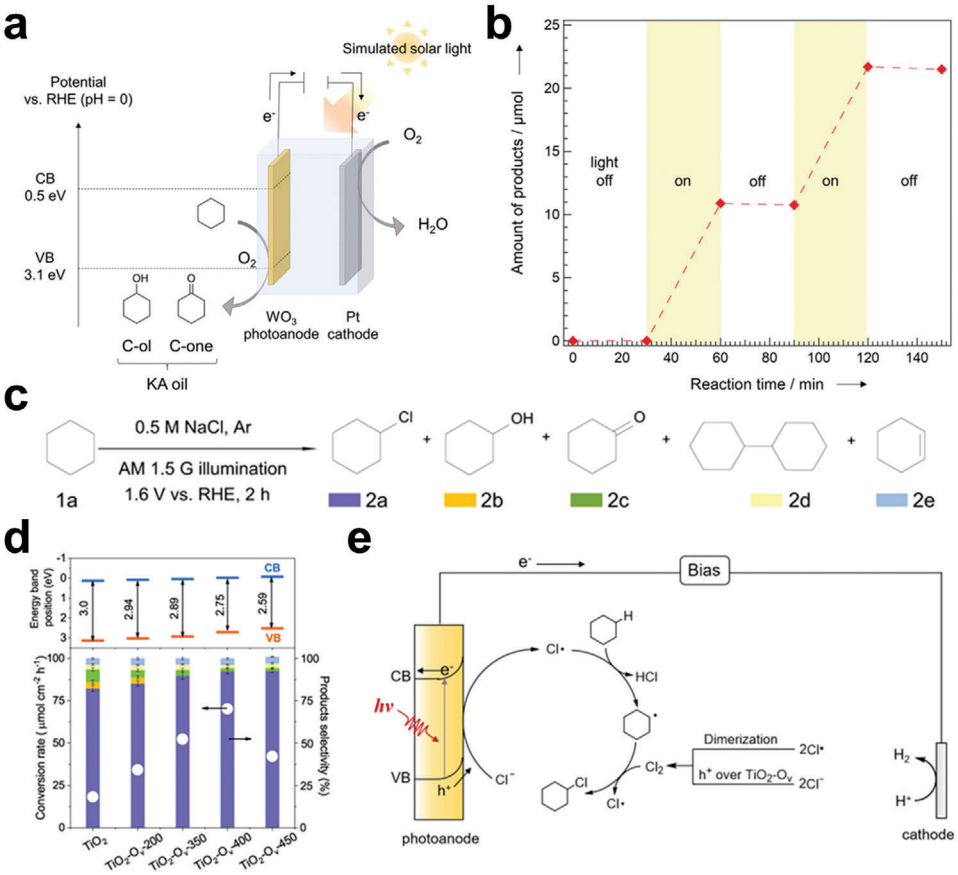

Figure 11. a) Schematic illustration of a PEC system for cyclohexane oxidation to produce KA oil. CB, VB, and RHE indicate the conduction band, valence band, and reversible hydrogen electrode, respectively. b) Effect of light irradiation on the PEC oxidation of cyclohexane to KA oil using a WO_3 electrode under air. Reproduced with permission.[149] Copyright 2018, Wiley-VCH. c) Conversion conditions of cyclohexane and the various expected products. d) Photoelectrocatalytic conversion rate of cyclohexane and the corresponding product selectivity over TiO_2-O_v-T (T represents the temperature in °C) photoanodes. e) Proposed mechanism of PEC chlorination of cyclohexane over the TiO_2-O_v-400 photoanode. Reproduced with permission.[45] Copyright 2021, Springer Nature.

challenging due to their high dissociation energy (438 kJ mol^{-1}). However, some recent success on electro and photocatalytic conversion of cyclohexane into KA oil has been performed, which provides a possibility of converting cyclohexane through PEC.[147,148] Tateno et al. utilized a porous WO_3 photoanode to oxidize cyclohexane and produce KA oil at room temperature and atmospheric pressure (**Figure 11**a).[149] Under a *tert*-butyl alcohol (tBuOH) and HNO_3 mixed electrolyte, remarkable partial oxidation selectivity (99%) and high FE (76%) were achieved, and the applied bias could be reduced by approximately 2 V upon illumination. Notably, KA oil was produced only under illumination, and dark electrolysis conditions showed negligible KA oil

production (Figure 11b). These results clearly demonstrated the unique advantage of the PEC system in cyclohexane oxidation reactions. Although progress made in the field of PEC conversion of cyclohexane is limited, engineering of semiconductor properties or electrolyte conditions might further enhance the productivity and selectivity of the reaction.

Along with cyclohexane, the oxidation of cyclohexene has also received attention since the oxidation of cyclohexene can produce cyclohexenone, a versatile compound that is used for pharmaceutical and fragrance applications. As mentioned above, Li et al. reported the oxidation of cyclohexene along with various other organic substrates by utilizing a $BiVO_4$ photoanode in organic media.[150] Upon adding mediators and co-oxidant organics in MeCN containing $LiClO_4$ electrolyte to drive the reaction, cyclohexene was successfully converted into cyclohexenone with a 38% yield after 8 h. Tateno et al. introduced N-hydroxyphthalimide (NHPI) as an electron transfer mediator, which oxidizes to form the phthalimide N-oxyl (PINO) radical, a useful catalyst for the abstraction of hydrogen from the C–H bond.[151] The NHPI/PINO mediator is advantageous for the activation of the stable C–H bond since it possesses a much higher oxidation potential than that of other mediators, such as TEMPO and NHSI. Utilizing a $WO_3/BiVO_4$ photoanode in MeCN containing $LiClO_4$ electrolyte, the onset potential was pulled approximately 1.0 V compared to electrochemical reactions, and constant-current photoelectrolysis at 0.1 mA cm^{-2} successfully oxidized cyclohexene to cyclohexenone with an FE close to 100%. Moreover, either alternating or removing the mediator resulted in decreased FE, which further supported the assumption that the NHPI/PINO mediator eliminated competing oxidation reactions.

In addition to oxidation, halogenative activation of the C–H bond can produce organic halides, a family of important chemicals with wide applications such as medicine, dyestuffs, and argochemicals. Since conventional halogenation requires thermal and toxic conditions and electrochemical halogenation requires not only organic solvents but also a large overpotential of 2.5 V versus RHE, PEC halogenation is a plausible candidate for the green halogenation of organic molecules.[152] Using NaX ($X = Cl^-$, Br^-, I^-) as the electrolyte, Li et al. demonstrated PEC C–H bond activation over an oxygen-vacancy rich TiO_2 photoanode, with cyclohexane as the model substrate (Figure 11c).[45] Since photoanodes with a valence band more positive than the oxidation potential of the halogen ions are theoretically capable of C–H bond halogenation, various photoanodes, such as TiO_2, WO_3, $BiVO_4$, and ZnO, were investigated, and among them, TiO_2 showed the highest conversion rate. H_2 treatment was conducted to create oxygen vacancies in TiO_2, and surprisingly, TiO_2 photoanodes with oxygen vacancies ($TiO_2{}^-O_v$) showed a highly increased conversion rate and product selectivity (Figure 11d). Mechanistic studies suggested that the oxygen vacancies acted as adsorption sites for halogen ions, in which they could be further oxidized into free radicals to participate in the halogenation process (Figure 11e). As a result, mono-halogenated cyclohexane was successfully produced with a selectivity of 92.5% and a production rate of 0.064 mmol cm^{-2} h^{-1}. Moreover, with the help of solar panels, a self-powered PEC system utilizing seawater as the chlorine source was constructed, which achieved a chlorocyclohexane production rate of 412 μmol h^{-1} with simultaneous H_2 production. Recent works on PEC cyclohexane oxidation and PEC cyclohexene oxidation to produce value-added chemicals are summarized in **Table 4**.

4. Conclusion and Perspectives

In this review, we summarize current advances in PEC upgrading of organics, such as methanol, ethanol, glycol, glycerol, and complex hydrocarbons including benzyl alcohol and HMF. Substituting the sluggish water oxidation reaction on the anode side with the organic upgrading reaction to higher values while also generating larger amounts of H_2 with lower operating potentials makes PEC organic upgrading a promising strategy for the production of both value-added products and H_2 fuel driven by solar energy. Although PEC upgrading of organic materials offers new opportunities for sustainable, inexpensive, and high-efficiency solar energy utilization, there still exist a number of challenges in obtaining desirable products with high selectivity and yield that need to be overcome in the near future.

First, a comprehensive understanding of each organic upgrading reaction mechanism is necessary. Similar to the case for glycerol oxidation, in which the activation of different hydroxyl groups led to different products, a thorough analysis of reaction intermediates and products synthesized during the upgrading reaction is important to realize selective PEC oxidation with high performance. In addition, because the currently explored reactants are limited, exploration of cheap carbon resources from biomass derivatives, organic feedstocks, and plastics is needed to broaden the field of application for the PEC organic upgrading process. Furthermore, in-depth investigation is required to understand each reaction pathway and mechanism for different reactants, which will help continue the advancement in designing catalysts and developing reaction systems.

Second, direct capture of photoinduced charges at the solid/liquid interface might cause an uncontrollable oxidation pathway, causing the organic material to be overoxidized to the corresponding acid, even CO_2 and H_2O. Developing a direct charge transfer pathway through oxidation agents, such as H_2O_2, HClO, and Br_2, is considered a promising approach to regulating the hole-coupled oxygen atom transfer process. For example, Li et al. have recently demonstrated efficient benzyl alcohol oxidation to benzaldehyde by boosting the formation rate of in situ produced H_2O_2.[153] Sargent group reported the ethylene and propylene epoxidations with a production selectivity of ≈97% by in situ produced HClO at nanostructured Pd electrocatalyst.[154] Liu et al. realized photoelectrochemical epoxidation of alkenes with conversion efficiency and selectivity up to 100% for bromide as an oxidizing medium.[155] In addition to the introduction of these oxidation agents, free radical-mediated organic transformation reactions can also be referred to, as ·OH, $\cdot O^{2-}$ and $^1O_2$ are probably realized by photoinduced charges.

Third, the aqueous PEC reaction is a heterogeneous catalysis process, and the reaction kinetics are partly dependent on the concentration of organic substrates. The complete upgrading of organic substrates to desirable products is hardly achieved. Ingenious reaction system design needs to be devoted, such as coupling organic dehydrogenation with proton reduction in pure organic electrolytes.

Table 4. List of value-added chemicals produced by PEC cyclohexane & cyclohexene conversion.

Catalyst	Light condition	Potential	Electrolyte	Main product	Selectivity [%]	Photocurrent [mA cm^{-2}]	Refs.
WO_3	AM 1.5G (100 mW cm^{-2})	0.5 V vs CE[a)]	18 mL cyclohexane 12 mL t-BuOH 2 mL HNO_3	KA oil	76	2[b)]	[149]
$BiVO_4$	AM 1.5G (100 mW cm^{-2})	0.996 V vs RHE	0.5×10^{-3} M cyclohexene MeCN 0.1 M $LiClO_4$ 2×10^{-3} M pyridine 0.2×10^{-3} M NHS 1.5×10^{-3} M t-BuOOH	cyclohexenone	–	1.2[b)]	[150]
$BiVO_4/WO_3$	AM 1.5G (100 mW cm^{-2})	- [c)]	10×10^{-3} M cyclohexene MeCN 0.1 M $LiClO_4$ 10×10^{-3} M NHPI	2-cyclohexene-1-one	>99	0.1	[151]
TiO_2-O_v	AM 1.5G (100 mW cm^{-2})	1.6 V vs RHE	18.8×10^{-3} M cyclohexane 0.5 M NaCl (pH 7)	Chlorocyclohexane	88.6	4.6	[45]

[a)] Counter electrode; [b)] Approximately estimated; [c)] Photocurrents were measured under constant-current mode.

Except for the above challenges originating from organic catalysis, tuning the photoelectrode texture, including facets, components, surface properties, and nanostructures, or introducing well-defined cocatalysts, such as Ni-based hydroxide for alcohol dehydrogenation, are also considered to be effective for selectively regulating the thermodynamic or kinetic processes of organic upgrading toward high product yields.

Finally, designing and optimizing large-area PEC cells with inlet and outlet streamlines is essential to improve the organic upgrading process, especially in scaling up the system. Light absorption ability and the separation of the products are important factors to be considered when designing PEC photoelectrodes. Most PEC reactions on a small laboratory scale have been conducted using single or H-type cells, which are still challenging to perform due to the inability to promote productivity and efficiently separate products. In addition, different from conventional water oxidizing reactions, organic reactants may have colors that affect the intensity of induced light into photoanodes, or they may exhibit high viscosity, which may show sluggish mass transfer, resulting in lowered efficiency of the photoanodes. Therefore, seeking suitable PEC cells designed for specific conditions is required to establish PEC organic upgrading reactions toward higher profit.

Overall, PEC organic transformation presents a tunable reaction pathway, direct oxidation by photogenerated hole transfer and indirect oxidation by various oxidant species, respectively, which is moving toward intelligentization and miniaturization systems to produce different target production. It is therefore expected that the PEC reaction can not only update the small organic molecular towards high-value-added chemicals but also offer the chance for biomass reforming and plastic recycling. Such efforts on photoanodes, with the simultaneous H_2 production at cathodes, will have the potential to gain economic advantage and lead to the implementation of PEC processes in the real industry in the near future.

Acknowledgements

T.-K.L., G.Y.J., and S.K. contributed equally to this work. This work was supported by Yonsei–KIST convergence research program and Yonsei Fellow Program (Lee Youn Jae). X.L.Z. thanks the National Science Foundation EFRI–DCheM program (Agreement: SUB0000425), and Stanford Natural Gas Initiative for their generous support. This work was also supported by NRF Korea (NRF-2019R1A2C3010479).

Conflict of Interest

The authors declare no conflict of interest.

Keywords

high value, organic conversion, organic syntheses, organic upgrading, photoelectrochemistry, value-added chemicals

Received: March 10, 2023
Revised: May 22, 2023
Published online:

[1] M. Grätzel, *Nature* **2001**, *414*, 338.
[2] Z. Li, W. Luo, M. Zhang, J. Feng, Z. Zou, *Energy Environ. Sci.* **2013**, *6*, 347.
[3] J. Li, N. Wu, *Catal. Sci. Technol.* **2015**, *5*, 1360.
[4] X. Shi, L. Cai, M. Ma, X. Zheng, J. H. Park, *ChemSusChem* **2015**, *8*, 3192.
[5] K. Sivula, R. van de Krol, *Nat. Rev. Mater.* **2016**, *1*, 15010.
[6] A. J. Bard, M. A. Fox, *Acc. Chem. Res.* **1995**, *28*, 141.
[7] A. J. Bard, *Science* **1980**, *207*, 139.
[8] T. Hisatomi, J. Kubota, K. Domen, *Chem. Soc. Rev.* **2014**, *43*, 7520.
[9] H. L. Ngo, D. K. Mishra, V. Mishra, C. C. Truong, *Chem. Eng. Sci.* **2021**, *229*, 37.

[10] H. Lin, S. Luo, H. Zhang, J. Ye, *Joule* **2022**, *6*, 294.
[11] A. Fujishima, K. Honda, *Nature* **1972**, *238*, 37.
[12] R. van de Krol, *Principles of Photoelectrochemical Cells*, Springer Science, New York **2012**.
[13] J. R. Swierk, T. E. Mallouk, *Chem. Soc. Rev.* **2013**, *42*, 2357.
[14] H. Zhang, H. Wang, J. Xuan, *J. Power Sources* **2020**, *462*, 228113.
[15] S. Haussener, C. Xiang, J. M. Spurgeon, S. Ardo, N. S. Lewis, A. Z. Weber, *Energy Environ. Sci.* **2012**, *5*, 9922.
[16] M. Z. Iqbal, S. Siddique, *Int. J. Hydrogen Energy* **2018**, *43*, 21502.
[17] A. Y. R. Ng, B. Boruah, K. F. Chin, J. M. Modak, H. S. Soo, *ChemNanoMat* **2020**, *6*, 185.
[18] M. Yamamoto, K. Tanaka, *ChemPlusChem* **2016**, *81*, 1028.
[19] F. Niu, D. Wang, L. J. Williams, A. Nayak, F. Li, X. Chen, L. Troian-Gautier, Q. Huang, Y. Liu, M. K. Brennaman, J. M. Papanikolas, L. Guo, S. Shen, T. J. A. Meyer, *Chemistry* **2022**, *28*, e202102630.
[20] S. Kim, K. H. Kim, C. Oh, K. Zhang, J. H. Park, *Carbon Energy* **2022**, *4*, 21.
[21] A. Grimaud, O. Diaz-Morales, B. Han, W. T. Hong, Y.-L. Lee, L. Giordano, K. A. Stoerzinger, M. T. M. Koper, Y. Shao-Horn, *Nat. Chem.* **2017**, *9*, 457.
[22] W. T. Hong, K. A. Stoerzinger, Y.-L. Lee, L. Giordano, A. Grimaud, A. M. Johnson, J. Hwang, E. J. Crumlin, W. Yange, T. Shao-Horn, *Energy Environ. Sci.* **2017**, *10*, 2190.
[23] T. Reier, H. N. Nong, D. Teschner, R. Schlögl, P. Strasser, *Adv. Energy Mater.* **2017**, *7*, 1601275.
[24] L. Bai, S. Lee, X. Hu, *Angew. Chem., Int. Ed.* **2021**, *60*, 3095.
[25] J. Song, C. Wei, Z.-F. Huang, C. Liu, L. Zeng, X. Wang, Z. J. Xu, *Chem. Soc. Rev.* **2020**, *49*, 2196.
[26] S. Y. Chae, E. D. Park, *Appl. Surf. Sci.* **2022**, *583*, 152566.
[27] H. Zhao, X. Li, M. Cai, C. Liu, Y. You, R. Wang, A. I. Channa, F. Lin, D. Huo, G. Xu, X. Tong, Z. M. Wang, *Adv. Energy Mater.* **2021**, *11*, 2101230.
[28] D. Li, J. Shi, C. Li, *Small* **2018**, *14*, 17014179.
[29] J. P. Barham, B. König, *Angew. Chem., Int. Ed.* **2020**, *59*, 11732.
[30] L. Buglioni, F. Raymenants, A. Slattery, S. D. A. Zondag, T. Noël, *Chem. Rev.* **2022**, *122*, 2752.
[31] K. Zhang, J. Liu, L. Wang, B. Jin, X. Yang, S. Zhang, J. H. Park, *J. Am. Chem. Soc.* **2020**, *142*, 8641.
[32] C. Dong, Y. Yang, X. Hu, Y. Cho, G. Jang, Y. Ao, L. Wang, J. Shen, J. H. Park, K. Zhang, *Nat. Commun.* **2022**, *13*, 4982.
[33] X. Shi, Y. Zhang, S. Siahrostami, X. Zheng, *Adv. Energy Mater.* **2018**, *8*, 1801158.
[34] M. S. Koo, X. Chen, K. Cho, T. An, W. Choi, *Environ. Sci. Technol.* **2019**, *53*, 9926.
[35] S. Iguchi, Y. Miseki, K. Sayama, *Sustainable Energy Fuels* **2018**, *2*, 155.
[36] M. T. Bender, X. Yuan, K.-S. Choi, *Nat. Commun.* **2020**, *11*, 4594.
[37] P. Li, T. Zhang, M. A. Mushtaq, S. Wu, X. Xiang, D. Yan, *Chem. Rec.* **2021**, *21*, 841.
[38] Y.-C. Wu, R.-J. Song, J.-H. Li, *Org. Chem. Front.* **2020**, *7*, 1895.
[39] S. D. Tilley, *Adv. Energy Mater.* **2019**, *9*, 1802877.
[40] K. Sivula, *J. Phys. Chem. Lett.* **2013**, *4*, 1624.
[41] M. D. Bhatt, J. S. Lee, *J. Mater. Chem. A* **2015**, *3*, 10632.
[42] C. C. Dorris, E. Lu, S. Park, F. H. Toro, *CBE: Life Sci. Educ. Working paper*, University of Pennsylvania, **2016**, https://repository.upenn.edu/cbe_sdr/78/
[43] Y. Li, X. Wei, L. Chen, J. Shi, *Angew. Chem., Int. Ed.* **2021**, *60*, 19550.
[44] Y. Zhao, C. Deng, D. Tang, L. Ding, Y. Zhang, H. Sheng, H. Ji, W. Song, W. Ma, C. Chen, J. Zhao, *Nat. Catal.* **2021**, *4*, 684.
[45] Z. Li, L. Luo, M. Li, W. Chen, Y. Liu, J. Yang, S. M. Xu, H. Zhou, L. Ma, M. Xu, X. Kong, H. Duan, *Nat. Commun.* **2021**, *12*, 6698.
[46] K. H. Ng, L. J. Minggu, W. F. Mark-Lee, K. Arifin, M. H. H. Jumali, M. B. Kassim, *Mater. Res. Bull.* **2018**, *98*, 47.
[47] N. Alenzi, W.-S. Liao, P. S. Cremer, V. Sanchez-Torres, T. K. Wood, C. Ehlig-Economides, Z. Cheng, *Int. J. Hydrogen Energy* **2010**, *35*, 11768.
[48] J. K. Kim, K. Shin, S. G. Cho, T.-W. Lee, J. H. Park, *Energy Environ. Sci.* **2011**, *4*, 1465.
[49] J. M. Spurgeon, N. Theaker, C. A. Phipps, S. S. Uttarwar, C. A. Grapperhaus, *ACS Sustainable Chem. Eng.* **2022**, *10*, 12882.
[50] ChemAnalyst, Decode the Future of Formaldehyde, chemanalyst.com/industry-report/formaldehyde-market-627 (accessed: February 2023).
[51] L.-W. Huang, T.-G. Vo, C.-Y. Chiang, *Electrochim. Acta* **2019**, *322*, 134725.
[52] K. Shimura, H. Yoshida, *Energy Environ. Sci.* **2011**, *4*, 2467.
[53] N. Hykaway, W. M. Sears, H. Morisaki, S. R. Morrison, *J. Phys. Chem.* **1986**, *90*, 6663.
[54] P. Lianos, *J. Hazard. Mater.* **2011**, *185*, 575.
[55] P. Solt, J. Konnerth, W. Gindl-Altmutter, W. Kantner, J. Moser, R. Mitter, H. W. G. van Herwijnen, *Int. J. Adhes. Adhes.* **2019**, *94*, 99.
[56] L. Zhang, *Formaldehyde: Exposure, Toxicity and Health Effects*, Royal Society of Chemistry, London **2018**.
[57] K. E. Hovda, K. McMartin, D. Jacobsen, *Rev. Chem. Eng.* **2014**, *30*, 583.
[58] L. E. Heim, H. Konnerth, M. H. G. Prechtl, *Green Chem.* **2017**, *19*, 2347.
[59] G. J. Millar, M. Collins, *Ind. Eng. Chem. Res.* **2017**, *56*, 9247.
[60] H. Adkins, W. R. Peterson, *J. Am. Chem. Soc.* **1931**, *53*, 1512.
[61] T. Osaka, K. Ejiri, N. Hirota, *J. Electrochem. Soc.* **1984**, *131*, 1571.
[62] T. Nash, *Biochem. J.* **1953**, *55*, 416.
[63] J. Marugán, R. van Grieken, C. Pablos, C. Adán, R. Timmers, *Int. J. Chem. React. Eng.* **2013**, *11*, 787.
[64] C. Haisch, J. Schneider, M. Fleisch, H. Gutzmann, T. Klassen, D. W. Bahnemann, *Dalton Trans.* **2017**, *46*, 12811.
[65] C. A. Mesa, A. Kafizas, L. Francás, S. R. Pendlebury, E. Pastor, Y. Ma, J. R. Durrant, *J. Am. Chem. Soc.* **2017**, *139*, 11537.
[66] T. Berger, T. Lana-Villarreal, D. Monllor-Satoca, R. Gómez, *J. Phys. Chem. C* **2008**, *112*, 15920.
[67] B.-F. Zheng, T. Ouyang, Z. Wang, J. Long, Y. Chen, Z.-Q. Liu, *Chem. Commun.* **2018**, *54*, 9583.
[68] S. Huang, T. Ouyang, B.-F. Zheng, Z.-Q. Liu, *Angew. Chem., Int. Ed.* **2021**, *60*, 9546.
[69] S. Huang, B.-F. Zheng, Z.-Y. Tang, X.-Q. Mai, T. Ouyang, Z.-Q. Liu, *Chem. Eng. J.* **2021**, *422*, 130086.
[70] S. Huang, F. Feng, R.-T. Huang, J. Liu, Z.-Q. Liu, *Adv. Mater.* **2022**, *34*, 2208438.
[71] J. Hietala, A. Vuori, P. Johnsson, I. Pollari, W. Reutemann, H. Kieczka, *Ullmann's Encyclopedia of Industrial Chemistry*, 6th ed, Wiley-VCH, Weinheim, Germany **2016**.
[72] D. A. Bulushev, J. R. H. Ross, *ChemSusChem* **2018**, *11*, 821.
[73] J. Eppinger, K.-W. Huang, *ACS Energy Lett.* **2017**, *2*, 188.
[74] C.-Y. Lin, Y.-C. Chueh, C.-H. Wu, *Chem. Commun.* **2017**, *53*, 7345.
[75] S.-C. Huang, C.-C. Cheng, Y.-H. Lai, C.-Y. Lin, *Chem. Eng. J.* **2020**, *395*, 125176.
[76] Y. Guan, E. J. M. Hensen, *J. Catal.* **2013**, *305*, 135.
[77] H. Xiang, R. Xin, N. Prasongthum, P. Natewong, T. Sooknoi, J. Wang, P. Reubroycharoen, X. Fan, *Resour. Chem. Mater.* **2022**, *1*, 47.
[78] P. M. Adamopoulos, I. Papagiannis, D. Raptis, P. Lianos, *Catalysts* **2019**, *9*, 976.
[79] M. Antoniadou, P. Bouras, N. Strataki, P. Lianos, *Int. J. Hydrogen Energy* **2008**, *33*, 5045.
[80] E. Doukas, P. Balta, D. Raptis, G. Avgouropoulos, P. Lianos, *Materials* **2018**, *11*, 1269.
[81] T. Takei, N. Iguchi, M. Haruta, *Catal. Surv. Asia* **2011**, *15*, 80.

[82] L. R. Lynd, X. Liang, M. J. Biddy, A. Allee, H. Cai, T. Foust, M. E. Himmel, M. S. Laser, M. Wang, C. E. Wyman, *Curr. Opin. Biotechnol.* **2017**, *45*, 202.
[83] B. R. Müller, S. Majoni, R. Memming, D. Meissner, *J. Mater. Chem. B* **1997**, *14*, 2501.
[84] C. Ampelli, F. Tavella, C. Genovese, S. Perathoner, M. Favaro, G. Centi, *J. Energy Chem.* **2017**, *26*, 284.
[85] J. Boltersdorf, A. C. Leff, G. T. Forcherio, D. R. Baker, *Crystals* **2021**, *11*, 226.
[86] J. Yuan, Y. Yuan, J. Zhang, H. Xu, Z. Mao, Y. Ma, *ChemSusChem* **2022**, *15*, 202102313.
[87] H. Yue, Y. Zhao, X. Ma, J. Gong, *Chem. Soc. Rev.* **2012**, *41*, 4218.
[88] A. Launay, F. Thominette, J. Verdu, *Polym. Degrad. Stab.* **1994**, *46*, 319.
[89] S. Ügdüler, K. M. van Geem, R. Denolf, M. Roosen, N. Mys, K. Ragaert, S. De Meester, *Green Chem.* **2020**, *22*, 5376.
[90] H. Zhou, Y. Ren, Z. Li, M. Xu, Y. Wang, R. Ge, X. Kong, L. Zheng, H. Duan, *Nat. Commun.* **2021**, *12*, 4679.
[91] J. Wang, X. Li, M. Wang, T. Zhang, X. Chai, J. Lu, T. Wang, Y. Zhao, D. Ma, *ACS Catal.* **2022**, *12*, 6722.
[92] C.-Y. Lin, S.-C. Huang, Y.-G. Lin, L.-C. Hsu, C.-T. Yi, *Appl. Catal., B* **2021**, *296*, 120351.
[93] X. Li, J. Wang, T. Zhang, T. Wang, Y. Zhao, *ACS Sustainable Chem. Eng.* **2022**, *10*, 9546.
[94] X. Li, J. Wang, M. Sun, X. Qian, Y. Zhao, *J. Energy Chem.* **2023**, *78*, 487.
[95] M. H. Haider, N. F. Dummer, D. W. Knight, R. L. Jenkins, M. Howard, J. Moulijn, S. H. Taylor, G. J. Hutchings, *Nat. Chem.* **2015**, *7*, 1028.
[96] M. Pagliaro, R. Ciriminna, H. Kimura, M. Rossi, C. D. Pina, *Angew. Chem., Int. Ed.* **2007**, *46*, 4434.
[97] N. Razali, A. Z. Abdullah, *Appl. Catal., A* **2017**, *543*, 234.
[98] C. A. G. Quispe, C. J. R. Coronado, J. A. Carvalho Jr, *Renewable Sustainable Energy Rev.* **2013**, *27*, 475.
[99] B. Katryniok, H. Kimura, E. Skrzyńska, J.-S. Girardon, P. Fongarland, M. Capron, R. Ducoulombier, N. Mimura, S. Paul, F. Dumeignil, *Green Chem.* **2011**, *13*, 1960.
[100] L. Ma, W. Lu, Z. Xia, J. Wen, *Biochem. Eng. J.* **2010**, *49*, 61.
[101] C. C. de Escobar, M. A. Lansarin, J. H. Z. dos Santos, M. D. Brandestini, *J. Sol-Gel Sci. Technol.* **2018**, *88*, 220.
[102] S. Bagheri, N. M. Julkapli, W. A. Yehye, *Renewable Sustainable Energy Rev.* **2015**, *41*, 113.
[103] G. S. Kumar, Y. Wee, I. Lee, H. J. Sun, X. Zhao, S. Xia, S. Kim, J. Lee, P. Wang, J. Kim, *Chem. Eng. J.* **2015**, *276*, 283.
[104] S.-S. Liu, K.-Q. Sun, B.-Q. Xu, *ACS Catal.* **2014**, *4*, 2226.
[105] EChemi, Guide of (±)-Glyceraldehyde, https://www.echemi.com/products/pid_Seven41083-dl-glyceraldehyde.html (accessed: February 2023).
[106] L. L. Nascimento, J. Z. Marinho, A. L. R. dos Santos, A. M. de Faria, R. A. C. Souza, C. Wang, A. O. T. Patrocinio, *Appl. Catal., A* **2022**, *626*, 118867.
[107] Y. Zhang, N. Zhang, Z.-R. Tang, Y.-J. Xu, *Chem. Sci.* **2013**, *4*, 1820.
[108] Q. Wang, X. Ma, P. Wu, B. Li, L. Zhang, J. Shi, *Nano Energy* **2021**, *89*, 106326.
[109] D. Liu, J.-C. Liu, W. Cai, J. Ma, H. B. Yang, H. Xiao, J. Li, Y. Xiong, Y. Huang, B. Liu, *Nat. Commun.* **2019**, *10*, 1779.
[110] W. Hu, D. Knight, B. Lowry, A. Varma, *Ind. Eng. Chem. Res.* **2010**, *49*, 10876.
[111] Y. Sun, G. Han, L. Du, C. Du, X. Zhou, Q. Sun, Y. Gao, G. Yin, Y. Li, Y. Wang, *Chem. Catal.* **2021**, *1*, 1260.
[112] L. Luo, W. Chen, S.-M. Xu, J. Yang, M. Li, H. Zhou, M. Xu, M. Shao, X. Kong, Z. Li, H. Duan, *J. Am. Chem. Soc.* **2022**, *144*, 7720.
[113] R. Tang, L. Wang, Z. Zhang, W. Yang, H. Xu, A. Kheradmand, Y. Jiang, R. Zheng, J. Huang, *Appl. Catal., B* **2021**, *296*, 120382.
[114] Y. Miao, Z. Li, Y. Song, K. Fan, J. Guo, R. Li, M. Shao, *Appl. Catal., B* **2023**, *323*, 122147.
[115] T.-G. Vo, C.-C. Kao, J.-L. Kuo, C.-C. Chiu, C.-Y. Chiang, *Appl. Catal., B* **2020**, *278*, 119303.
[116] J. Ouyang, X. Liu, B.-H. Wang, J.-B. Pan, S. Shen, L. Chen, C.-T. Au, S.-F. Yin, *ACS Appl. Mater. Interfaces* **2022**, *14*, 23536.
[117] G. Dodekatos, S. Schünemann, H. Tüysüz, *ACS Catal.* **2018**, *8*, 6301.
[118] Y. Liu, M. Wang, B. Zhang, D. Yan, X. Xiang, *ACS Catal.* **2022**, *12*, 6946.
[119] J. Yu, J. González-Cobos, F. Dappozze, F. J. López-Tenllado, J. Hidalgo-Carrillo, A. Marinas, P. Vernoux, A. Caravaca, C. Guillard, *Appl. Catal., B* **2022**, *318*, 121843.
[120] Z. Gu, X. An, R. Liu, L. Xiong, J. Tang, C. Hu, H. Liu, J. Qu, *Appl. Catal., B* **2021**, *282*, 119541.
[121] C. Lin, C. Dong, S. Kim, Y. Lu, Y. Wang, Z. Yu, Y. Gu, Z. Gu, D. K. Lee, K. Zhang, J. H. Park, *Adv. Mater.* **2023**, *35*, 2209955.
[122] Y. Lee, S. Kim, S. Y. Jeong, S. Seo, C. Kim, H. Yoon, H. W. Jang, S. Lee, *Catal. Today* **2021**, *359*, 43.
[123] Y.-H. Wu, D. A. Kuznetsov, N. C. Pflug, A. Fedorov, C. R. Müller, *J. Mater. Chem. A* **2021**, *9*, 6252.
[124] M. C. Markham, M. C. Hannan, R. M. Paternostro, C. B. Rose, *J. Am. Chem. Soc.* **1958**, *80*, 5394.
[125] W. Song, A. K. Vannucci, B. H. Farnum, A. M. Lapides, M. K. Brennaman, B. Kalanyan, L. Alibabaei, J. J. Concepcion, M. D. Losego, G. N. Parsons, T. J. Meyer, *J. Am. Chem. Soc.* **2014**, *136*, 9773.
[126] L. Bai, F. Li, Y. Wang, H. Li, X. Jiang, L. Sun, *Chem. Commun.* **2016**, *52*, 9711.
[127] Z. Zhou, Y.-N. Xie, W. Zhu, H. Zhao, N. Yang, G. Zhao, *Appl. Catal., B* **2021**, *286*, 119868.
[128] L. Luo, Z.-j. Wang, X. Xiang, D. Yan, J. Ye, *ACS Catal.* **2020**, *10*, 4906.
[129] R. Zhang, M. Shao, Z. Li, F. Ning, M. Wei, D. G. Evans, X. Duan, *Chemistry* **2017**, *23*, 8142.
[130] N. Karjule, R. S. Phatake, S. Barzilai, B. Mondal, A. Azoulay, A. I. Shames, M. Volokh, J. Albero, H. G. M. Shalom, *J. Mater. Chem. A* **2022**, *10*, 16585.
[131] J.-L. Zhuang, Y.-M. Shen, Y. Xue, M. Yan, H. Cheng, Z. Chen, X.-J. Yu, X.-B. Lian, S.-B. Zhu, *ACS Appl. Energy Mater.* **2020**, *3*, 9098.
[132] N. K. McMillan, D. A. Lopez, G. Leem, B. D. Sherman, *ChemPlusChem* **2022**, *87*, 202200187.
[133] E. Nikoloudakis, P. B. Pati, G. Charalmbidis, D. S. Budkina, S. Diring, A. Planchat, D. Jacquemin, E. Vauthey, A. G. Coutsolelos, F. Odobel, *ACS Catal.* **2021**, *11*, 12075.
[134] D. F. Bruggeman, S. Mathew, R. J. Detz, J. N. H. Reek, *Sustainable Energy Fuels* **2021**, *5*, 5707.
[135] D. F. Bruggeman, T. M. A. Bakker, S. Mathew, J. N. H. Reek, *Chemistry* **2021**, *27*, 218.
[136] A. Isogai, T. Hänninen, S. Fujisawa, T. Saito, *Prog. Polym. Sci.* **2018**, *86*, 122.
[137] Q. Shi, H. Duan, *Chem. Catal.* **2022**, *2*, 3471.
[138] J. Na, B. Seo, J. Kim, C. W. Lee, H. Lee, Y. J. Hwang, B. K. Min, D. K. Lee, H.-S. Oh, U. Lee, *Nat. Commun.* **2019**, *10*, 5193.
[139] X. M. C. Ta, R. Daiyan, T. K. A. Nguyen, R. Amal, T. T. Phu, A. Tricoli, *Adv. Energy Mater.* **2022**, *12*, 2201358.
[140] H. G. Cha, K. S. Choi, *Nat. Chem.* **2015**, *7*, 328.
[141] D. J. Chadderdon, L.-P. Wu, Z. A. McGraw, M. Panthani, W. Li, *ChemElectroChem* **2019**, *6*, 3387.
[142] C. R. Lhermitte, N. Plainpan, P. Canjura, F. Boudoire, K. Sivula, *RSC Adv.* **2021**, *11*, 198.
[143] U. Schuchardt, D. Cardoso, R. Sercheli, R. Pereira, R. S. da Cruz, M. C. Guerreiro, D. Mandelli, E. V. Spinacé, E. L. Pires, *Appl. Catal., A* **2001**, *211*, 1.

[144] EChemi, Guide of Cyclohexanone, https://www.echemi.com/productsInformation/pid_Seven3075-cyclohexanone.html (accessed: February 2023).
[145] EChemi, Guide of Cyclohexanol, https://www.echemi.com/productsInformation/pid_Seven3073-cyclohexanol.html (accessed: February 2023).
[146] W.-J. Zhou, R. Wischert, K. Xue, Y.-T. Zheng, B. Albela, L. Bonneviot, J.-M. Clacens, F. D. Campo, M. P. -Titus, P. Wu, *ACS Catal.* **2014**, *4*, 53.
[147] H. Tian, Y. Zhang, Z. Zhang, T. Lv, L. Bian, H. Wang, J. Li, Y. Yamauchi, Z.-L. Wang, *ChemCatChem* **2023**, *15*, 202201220.
[148] L. Xiang, J. Fan, W. Zhong, L. Mao, K. You, D. Yin, *Appl. Catal., A* **2019**, *575*, 120.
[149] H. Tateno, S. Iguchi, Y. Miseki, K. Sayama, *Angew. Chem., Int. Ed.* **2018**, *57*, 11238.
[150] T. Li, T. Kasahara, J. He, K. E. Dettelbach, G. M. Sammis, C. P. Berlinguette, *Nat. Commun.* **2017**, *8*, 390.
[151] H. Tateno, Y. Miseki, K. Sayama, *Chem. Commun.* **2019**, *55*, 9339.
[152] Y. Yuan, A. Yao, Y. Zheng, M. Gao, Z. Zhou, J. Qiao, J. Hu, B. Ye, J. Zhao, H. Wen, A. Lei, *iScience* **2019**, *12*, 293.
[153] H. Li, C. Lin, Y. Yang, C, D., Y. Min, X. Shi, L. Wang, S. Lu, K. Zhang, *Angew. Chem., Int. Ed.* **2023**, *135*, e202210804.
[154] W. R. Leow, Y. Lum, A. Ozden, Y. Wang, D.-H. Nam, B. Chen, J. Wicks, T.-T. Zhuang, F. Li, D. Sinton, E. H. Sargent, *Science* **2020**, *368*, 1228.
[155] X. Liu, Z. Chen, S. Xu, G. Liu, Y. Zhu, X. Yu, L. Sun, F. Li, *J. Am. Chem. Soc.* **2022**, *144*, 19770.

Tae-Kyung Liu is currently an integrated M.S./Ph.D. course student under the supervision of Prof. Jong Hyeok Park at the Department of Chemical and Biomolecular Engineering in Yonsei University, Republic of Korea. His research interests focus on the surface and interface engineering of nanomaterials for electrochemical and photoelectrochemical water splitting.

Gyu Yong Jang is currently an integrated M.S./Ph.D. course student under the supervision of Prof. Jong Hyeok Park at the Department of Chemical and Biomolecular Engineering in Yonsei University, Republic of Korea. His research interests focus on the surface and interface engineering of nanomaterials for electrochemical and photoelectrochemical energy harvesting.

Sungsoon Kim received his Ph.D. in the Department of Chemical and Biomolecular Engineering at Yonsei University, Republic of Korea, in 2023 under the supervision of Prof. Jong Hyeok Park. He is currently a postdoctoral researcher in Prof. Xiaolin Zheng's group at Stanford University. His research interests include the surface and interface engineering of nanomaterials for electrochemical and photoelectrochemical cells.

Kan Zhang is a professor in the School of Materials Science and Engineering at Nanjing University of Science and Technology, P. R. China. He received his Ph.D. from the Institute of Nano Science and Technology at Sungkyunkwan University in February 2015. Then, he joined Yonsei University as a postdoctoral researcher in 2015 (under Prof. Jong Hyeok Park). In February 2018, he joined Nanjing University of Science and Technology as a professor and was awarded the distinguished professor of Jiangsu Province in 2020. His research focuses on photoelectrochemical water splitting, the directed transformation of small organic molecules coupled with hydrogen production, and photo-Fenton-like catalysis.

Xiaolin Zheng is a professor in the Department of Mechanical Engineering at Stanford University. She received her Ph.D. in mechanical and aerospace engineering from Princeton University in February 2006. Prior to joining Stanford in 2007, she conducted postdoctoral work in the Department of Chemistry and Chemical Biology at Harvard University. She received the TR35 Award from the MIT Technology Review (2013) and the Presidential Early Career Award (PECASE) from the White House (2009). Her research focuses on water electrolysis, machine learning for material design, combustion of energetic materials, and silicon nanowires for energy and environmental applications.

Jong Hyeok Park is a professor at the Department of Chemical and Biomolecular Engineering at Yonsei University, Republic of Korea. He received his Ph.D. in chemical engineering from KAIST, Republic of Korea, in August 2004. Then, he joined the University of Texas at Austin, as a postdoctoral researcher in 2004 (under Prof. Allen J. Bard). From March 2007 to February 2008, he worked at ETRI. He is an author and a coauthor of more than 350 papers and 50 patents. His research focuses on solar-to-hydrogen conversion devices, Li and Na ion batteries, and perovskite solar cells.